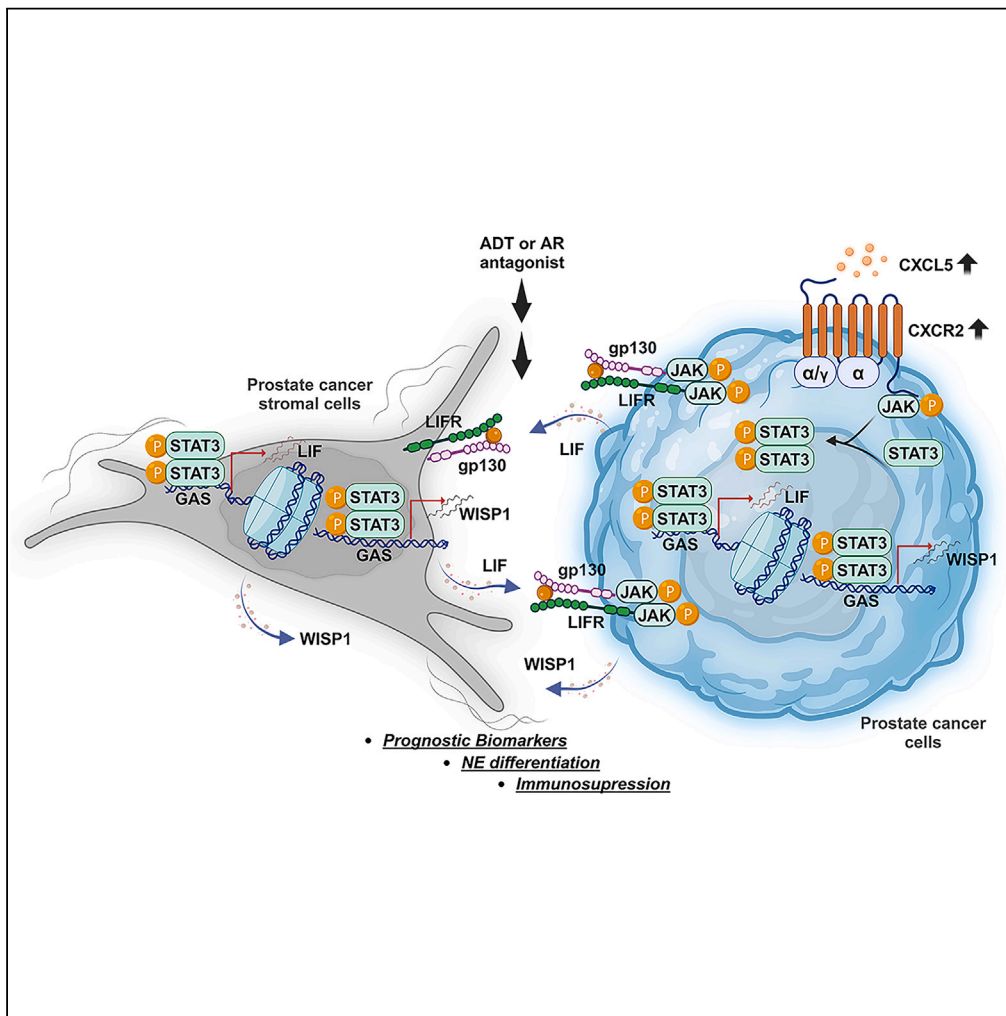# iScience

Article

WNT1-inducible signaling pathway protein 1 activation through C-X-C motif chemokine ligand 5/C-X-C chemokine receptor type 2/leukemia inhibitory factor/leukemia inhibitory factor receptor signaling promotes immunosuppression and neuroendocrine differentiation in prostate cancer

Ke Hung Tsui, Chien-Liang Liu, Hsiu-Lien Yeh, ..., Michael Hsiao, Wassim Abou-Kheir, Yen-Nien Liu

liuy@tmu.edu.tw

Highlights

PCa and stromal cells form an immunosuppressive TME, aiding tumor growth and evasion

CXCL5/CXCR2 and LIF/LIFR pathways loop, promoting NED and increasing WISP1

WISP1 upregulation induces immune checkpoints via LIF/LIFR and STAT3 activation

WISP1 levels in patient sera correlate with PCa progression, suggesting a biomarker

CellPress
OPEN ACCESS

Article

WNT1-inducible signaling pathway protein 1 activation through C-X-C motif chemokine ligand 5/C-X-C chemokine receptor type 2/leukemia inhibitory factor/leukemia inhibitory factor receptor signaling promotes immunosuppression and neuroendocrine differentiation in prostate cancer

Ke Hung Tsui,[1,2,7] Chien-Liang Liu,[3,7] Hsiu-Lien Yeh,[4] Ming-Kun Liu,[4] Chien-Hsiu Li,[1] Wei-Hao Chen,[4] Kuo-Ching Jiang,[4] Han-Ru Li,[4] Phan Vu Thuy Dung,[4] Michael Hsiao,[5] Wassim Abou-Kheir,[6] and Yen-Nien Liu[4,8,*]

SUMMARY

The interaction between prostate cancer (PCa) cells and prostate stromal cells fosters an immunosuppressive tumor microenvironment (TME) that promotes tumor growth and immune evasion. However, the specific signaling pathways involved remain unclear. We identified a key mechanism involving the CXCL5/CXCR2 and LIF/LIFR pathways, which create a feedforward loop that enhances neuroendocrine differentiation (NED) in PCa cells and upregulates WNT1-inducible signaling pathway protein 1 (WISP1) in both cell types. WISP1 upregulation is essential for inducing immune checkpoints and immunosuppressive cytokines via LIF/LIFR signaling and STAT3 phosphorylation. This process leads to increased neuroendocrine markers, immune checkpoints, cell proliferation, and migration. Notably, WISP1 levels in patient sera correlate with PCa progression, suggesting its potential as a biomarker. Our findings elucidate the mechanisms by which reciprocal communication between PCa cells and stromal cells contributes to the formation of an immunosuppressive TME, driving the malignant progression of PCa and highlighting potential targets for therapeutic intervention.

INTRODUCTION

The incidence and mortality of prostate cancer (PCa) are rapidly increasing among men worldwide.[1] While initial androgen-deprivation therapy (ADT) may bring improvements, some patients experience relapse and develop castration-resistant PCa (CRPC).[2] To address advanced PCa or CRPC, various treatment approaches have been employed, including hormone therapy, androgen receptor (AR) signaling blockade, and nonspecific chemotherapy. However, the prolonged inhibition of AR signaling often triggers a shift in disease progression, leading to a particularly lethal form known as neuroendocrine PCa (NEPC) in approximately 10%–20% of CRPC cases.[3] NEPC is associated with an unfavorable prognosis and is typically suspected when prostate-specific antigen (PSA) values are low but demonstrate worsening trends upon radiographic and clinical progression.[4] Unfortunately, there is currently a lack of effective therapeutic strategies specifically tailored to address NEPC. This highlights an urgent and unmet need to develop a groundbreaking treatment modality that can revolutionize the management of patients with NEPC.

In various types of cancer, cancer-associated fibroblasts (CAFs) were found to exhibit the elevated expression of C-X-C motif chemokine ligand 5 (CXCL5), which in turn promotes the expression of programmed cell death ligand 1 (PDL1) in tumor cells and contributes to the formation of an immunosuppressive tumor microenvironment (TME).[5] Tumor-associated macrophages (TAMs) expressing C-X-C chemokine receptor type 2 (CXCR2) strongly infiltrate and, upon activation by CXCL2, induce macrophage polarization toward an anti-inflammatory phenotype in *pten*-null prostate tumors.[6] CXCR2 is a prototypical G-protein-coupled receptor (GPCR) that was identified as a key driver of

[1]Department of Urology, Shuang Ho Hospital, Taipei Medical University, Taipei 110, Taiwan
[2]Department of Urology, School of Medicine, College of Medical, Taipei Medical University, Taipei 110, Taiwan
[3]Department of Surgery, Division of Urology, Chi Mei Medical Center, Tainan 710, Taiwan
[4]Graduate Institute of Cancer Biology and Drug Discovery, College of Medical Science and Technology, Taipei Medical University, Taipei 110, Taiwan
[5]Genomics Research Center, Academia Sinica, Taipei 115, Taiwan
[6]Department of Anatomy, Cell Biology and Physiological Sciences Faculty of Medicine, American University of Beirut, Beirut 1107-2020, Lebanon
[7]These authors contributed equally
[8]Lead contact
*Correspondence: liuy@tmu.edu.tw
https://doi.org/10.1016/j.isci.2024.110562

neuroendocrine differentiation (NED) in PCa.[7] The CXCL5/CXCR2 axis plays a critical role in immune cell recruitment, angiogenesis, tumor growth, and metastasis.[8] Despite the knowledge that CXCR2-activated signal transducer and activator of transcription 3 (STAT3) enhances the activation of the mitogen-activated protein kinase (MAPK) pathway,[9] the precise mechanism by which CXCL5/CXCR2 activates STAT3 to promote NED in PCa remains to be elucidated.

Prostate stromal cells play a crucial role in supporting the growth, development, and normal function of the prostate gland.[10] Interactions between prostate stromal cells and cancer cells, including the production of interleukin (IL)-6, create a dynamic and complex TME that contributes to tumor progression, therapy resistance, and evasion of immune responses.[11] Elevated levels of IL-6 are commonly observed in CRPC and were shown to decrease AR expression while inducing NED through the activation of the Janus tyrosine kinase 2 (JAK2)/STAT3 signaling pathway.[12] In our previous study, we identified that leukemia inhibitory factor (LIF), a member of the IL-6 cytokine family, is overexpressed in PCa cells undergoing NED after ADT.[13] Furthermore, we demonstrated that the activation of LIF and its receptor (LIFR) contributes to metabolic reprogramming and the induction of NED in PCa.[14] Despite this knowledge, the precise mechanism through which LIF/LIFR promotes NED and facilitates interactions between tumor cells and prostate stromal cells, resulting in an immunosuppressive response within the PCa TME, remains unclear.

WISP1 (WNT1-inducible signaling pathway protein 1), also known as CCN4, is a matricellular protein that plays a role in various biological processes, including cell proliferation, migration, and extracellular matrix remodeling.[15] In the context of PCa, WISP1 was found to be upregulated in both cancer cells and surrounding stromal cells.[16] WISP1 can modulate the immune response within the prostate TME.[17] It was shown to influence the recruitment and activation of immune cells, regulate the secretion of anti-inflammatory cytokines, create an immunosuppressive environment in melanomas.[18] The upregulation of WISP1 in prostate stromal cells was associated with tumor progression,[17,19,20] while the abundance of WISP1 drives the immunosuppressive microenvironment and the NED progression of PCa following ADT remains unclear. Therefore, our study aimed to investigate the regulatory mechanism underlying how ADT stimulates WISP1 in the TME, thereby enhancing the immunosuppressive response and promoting tumorigenesis in PCa.

RESULTS

Androgen-deprivation therapy induces C-X-C motif chemokine ligand 5, which promotes C-X-C chemokine receptor type 2-driven neuroendocrine differentiation of prostate cancer

We analyzed the baseline expression of CXCL5 and CXCR2 in various PCa cell lines, including AR-positive cells (LNCaP, C4-2, and 22Rv1), AR-negative cells (PC3), and the NEPC cell line LASCPC-01. Our observations revealed differential expression levels of CXCL5 and CXCR2, with the NEPC cell line LASCPC-01 exhibiting significantly elevated levels compared to AR-positive cells (Figure 1A). To investigate the impact of ADT on NED in PCa cells, we utilized androgen-dependent LNCaP cells treated with charcoal-stripped serum (CSS)-containing medium as a model for ADT. We found that CXCL5 levels increased in a time-dependent manner after treatment with a CSS-containing medium, accompanied by the upregulation of CXCR2 and a neuroendocrine marker (enolase 2 (ENO2)), while expressions of androgen-responsive markers (kallikrein 3 (KLK3) and NK3 homeobox 1 (NKX3-1)) decreased (Figure 1B). We also found a negative correlation between mRNA expression of CXCL5/CXCR2 and the androgen-responsive genes, KLK3 and NXK3-1, in a microarray dataset of LNCaP cells cultured in CSS-containing medium at different time points (GDS3358, Figure 1C). Moreover, LNCaP cells cultured in CSS-containing medium exhibited increased mRNA levels of CXCL5, CXCR2, and neuroendocrine markers, along with decreased expressions of androgen-responsive markers; however, treatment with the AR ligand, dihydrotestosterone (DHT), effectively counteracted the effects of ADT (Figure 1D). This confirmed the influence of ADT-induced CXCL5/CXCR2 signaling on NED progression. Consistently, overexpression of CXCL5 in LNCaP cells led to increased mRNA and protein levels of CXCR2 and neuroendocrine markers, while it reduced the levels of androgen-responsive markers. (Figures 1E and 1F). Moreover, the treatment of LNCaP and C4-2 cells with the recombinant CXCL5 protein led to increased mRNA and protein expressions of CXCR2 and neuroendocrine markers, while decreasing expressions of androgen-responsive markers (Figures 1G–1I). Notably, the effects of CXCL5 treatment were reversed when the CXCR2 inhibitor (navarixin) was administered (Figures 1G–1I). Furthermore, through a gene set enrichment analysis (GSEA) using the cancer genome atlas program (TCGA) PCa dataset, we observed that high expression levels of CXCL5 in tissues were associated with the upregulation of a NEPC-responsive gene signature (Li, Figure 1J) and the downregulation of androgen-responsive gene signatures (PID, Wang, Nelson, Hallmark, and GO, Figure 1K). Taken together, these findings suggest that the activation of the CXCL5/CXCR2 pathway plays a critical role in inducing NED in PCa after ADT. Inhibition of CXCR2 may serve as a potential strategy to suppress CXCL5-induced NED in PCa.

Involvement of the leukemia inhibitory factor in the C-X-C motif chemokine ligand 5/C-X-C chemokine receptor type 2 axis-driven neuroendocrine differentiation of prostate cancer

To investigate the involvement of CXCL5/CXCR2 expressions in microenvironmental variables of PCa, we conducted an analysis of associations between CXCL5/CXCR2 and cytokine-responsive gene signatures using TCGA PCa dataset. Through GSEAs, we observed that tissues expressing high levels of CXCL5 and CXCR2 were positively associated with gene signatures related to cytokine responsiveness (Figures S1A and S1B). Specifically, we focused on the top three gene signatures based on NESs. To further explore components of the cytokine response signature that were positively associated with the upregulated CXCL5/CXCR2 axis, we performed Venn diagram analyses. Seven and six genes were respectively observed to overlap in the top three cytokine response signatures in datasets with upregulated CXCL5 and CXCR2 (Figures S1C and S1D). To identify candidate genes correlated with CXCL5 and CXCR2, we conducted Pearson correlation analyses using TCGA dataset and identified six potential genes that exhibited positive correlations with CXCL5 and CXCR2 (Figures S1E and S1F).
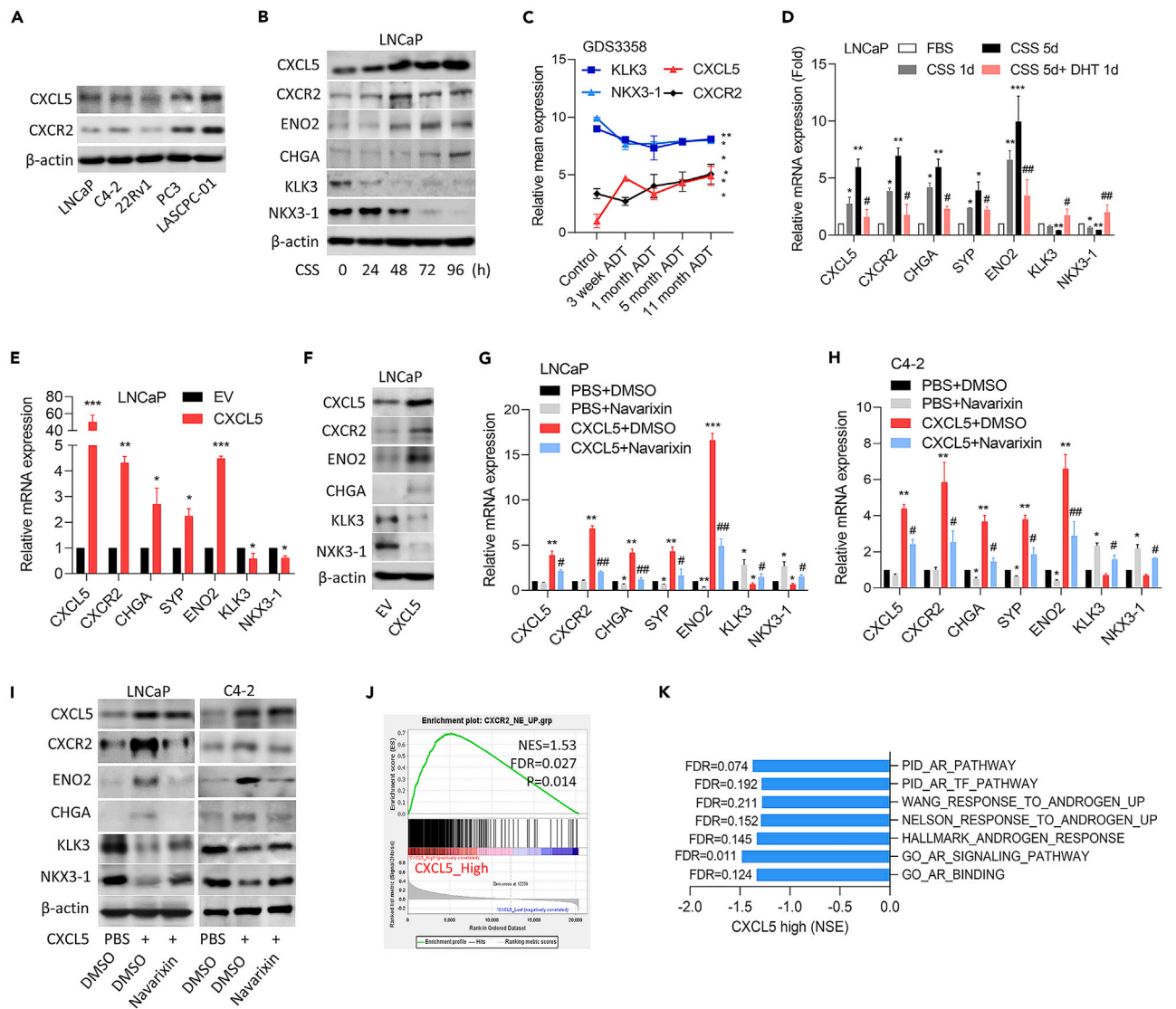
Figure 1. Androgen-deprivation therapy promotes CXCL5/CXCR2-driven neuroendocrine differentiation (NED) of prostate cancer (PCa)

(A) Relative protein levels of CXCL5 and CXCR2 in LNCaP, C4-2, 22Rv1, PC3, and LASCPC-01 cells.

(B) Relative protein levels of CXCL5, CXCR2, ENO2, CHGA, KLK3, and NKX3-1 in LNCaP cells cultured in CSS-containing medium for 0–96 h.

(C) Relative mean mRNA expression levels of *KLK3, NKX3-1, CXCL5*, and *CXCR2* in LNCaP cells from 3 weeks to 11 months of ADT in the GDS3358 database. * vs. Control, as determined by a one-way ANOVA.

(D) Relative mRNA levels of *CXCL5, CXCR2*, neuroendocrine (*CHGA, SYP*, and *ENO2*), and androgen-responsive (*KLK3* and *NKX3-1*) markers in LNCaP cells cultured in CSS-containing medium for 1 or 5 days, followed by treatment with 10 nM dihydrotestosterone (DHT) for 1 day * vs. FBS; # vs. CSS 5days, as determined by a two-way ANOVA.

(E) Relative mRNA levels of *CXCL5, CXCR2*, neuroendocrine, and androgen-responsive markers in LNCaP cells stably transfected with an empty vector (EV) or a CXCL5-expressing vector. * vs. EV, as determined by a one-way ANOVA.

(F) Relative protein levels of CXCL5, CXCR2, ENO2, CHGA, KLK3, and NKX3-1 in LNCaP cells stably expressing the EV or CXCL5-expressing vector.

(G and H) Relative mRNA levels of *CXCL5, CXCR2*, neuroendocrine, and androgen-responsive markers in LNCaP (G) and C4-2 (H) cells treated with PBS or 20 ng/mL of the CXCL5 recombinant protein, followed by treatment with DMSO or 5 μM navarixin for 48 h * vs. PBS+DMSO; # vs. CXCL5+DMSO, as determined by a one-way ANOVA.

(I) Relative protein levels of CXCL5, CXCR2, ENO2, CHGA, KLK3, and NKX3-1 in LNCaP and C4-2 cells treated with PBS or 20 ng/mL of the CXCL5 recombinant protein, followed by treatment with DMSO or 5 μM navarixin for 48 h.

(J) GSEA of the TCGA PCa dataset revealed a positive correlation between high CXCL5 expression in prostate tissues and gene signatures representing NEPC-response signaling (Li).

(K) GSEA of TCGA PCa dataset revealed an inverse correlation between high CXCL5 expression in prostate tissues and gene signatures representing androgen response signaling (PID, Wang, Nelson, Hallmark, and GO). NES, normalized enrichment score; FDR, false discovery rate. Quantification of relative mRNA levels is presented as the mean ± SEM from three biological replicates. *$p < 0.05$, **$p < 0.01$, ***$p < 0.005$.

Subsequently, we performed GSEAs on TCGA PCa dataset, examining abundances of *CXCL5* and *CXCR2* and using gene signatures associated with upregulated NEPC responsiveness (Beltran and Li). Among genes that overlapped in both NEPC gene signatures, the *LIF* showed the highest NES and a significant FDR of <0.15 (Figures S1G–S1I). It was reported that PCa cells abundant in CXCR2 expression are enriched in NEPC profiles.[7] We observed strong positive correlations in LIF-upregulated PCa samples with CXCR2-dependent NEPC-responsive gene signatures (Figure S1J). These findings suggested that the activation of CXCL5/CXCR2 axis-driven NED in PCa may be involved in LIF upregulation.

C-X-C motif chemokine ligand 5/C-X-C chemokine receptor type 2 signaling upregulates leukemia inhibitory factor expression via p-STAT3 binding to the gamma interferon activation site elements upstream of the leukemia inhibitory factor gene

To validate associations between CXCL5/CXCR2 signaling and responsive cytokines, we measured mRNA levels of six putative cytokines in CXCL5-expressing LNCaP cells. Our results revealed that the upregulation of *LIF*, *IL6*, *CSF3*, and *CCL3* was positively correlated with CXCR2 in cells overexpressing CXCL5 (Figure 2A). Similarly, the treatment of LNCaP and C4-2 cells with the recombinant CXCL5 protein resulted in increased levels of *LIF*, *IL6*, *CSF3*, and *CCL3*, which were positively associated with CXCR2 (Figures 2B and S2A). However, when a CXCR2 inhibitor was administered, *CXCR2*, *LIF*, and *IL6* expressions were reduced, while *CSF3* and *CCL3* levels remained unaffected (Figures 2B and S2A). We next performed immunoblots to assess protein levels and found that elevated CXCL5 protein levels were associated with increased LIF, LIFR, and p-STAT3 expressions (Figure 2C). Conversely, the treatment of CXCL5-treated cells with a CXCR2 inhibitor resulted in reduced protein levels of LIF, LIFR, and p-STAT3 (Figure 2D). These results suggested that the activation of CXCL5/CXCR2 signaling may promote LIF expression. To further investigate the binding of p-STAT3 to the *LIF* gene, we analyzed ChIP-sequencing data and identified multiple binding sites of STAT3 within the *LIF* gene (Figure 2E). We next searched for sequences resembling the GAS elements in the *LIF* regulatory sequence using the prediction of transcription factor-binding sites (PROMO) database of transcription factor-binding profiles,[21] and we identified five putative GAS elements upstream of the *LIF* transcription start site (Figure 2F). ChIP assays using an antibody against p-STAT3 were performed to assess binding capacities of GAS2, GAS3, and GAS5 on the *LIF* gene after CXCL5 protein treatment in LNCaP and C4-2 cells. Results showed that CXCL5 treatment significantly increased p-STAT3 binding to GAS2, GAS3, and GAS5 on the *LIF* gene, while CXCR2 inhibitor treatment decreased this binding capacity (Figures 2G and S2B). To validate the functional significance of these GAS elements, reporter assays were performed using a DNA construct containing either wild-type (WT)-GAS or mutant (M)-GAS sequences on the *LIF* regulatory sequence cloned into a GFP reporter (Figure 2F). Reporter gene activities of the WT-GAS2, WT-GAS3, and WT-GAS5 had significantly increased in CXCL5 protein-treated cells compared to untreated cells; however, reporter activity was reduced when CXCL5-treated cells were treated with a CXCR2 inhibitor (Figures 2H and S2C). Furthermore, M-GAS sequences (GAS2M, GAS3M, and GAS5M) on the *LIF* GFP-reporter showed reduced CXCL5-driven reporter gene activity in LNCaP and C4-2 cells (Figures 2I and S2D). These findings suggested that CXCL5/CXCR2-driven p-STAT3 may upregulate the *LIF* gene by directly binding to the GAS2, GAS3, and GAS5 regulatory sequences.

Leukemia inhibitory factor-driven neuroendocrine differentiation and malignant progression may occur through WNT1-inducible signaling pathway protein 1 activation in prostate cancer cells

Upregulation of the LIF influences the differentiation and polarization of macrophages, promoting the generation of anti-inflammatory TAMs, which are associated with tumor-promoting properties.[22] Understanding immune modulation mediated by the LIF is important for comprehending complex interactions between cancer cells and the immune system within the TME. Elevated WISP1 expression in PCa was associated with more-aggressive disease characteristics, including higher Gleason scores, advanced stages, and increased risks of recurrence.[19] To investigate whether LIF/LIFR signaling-driven NED and immune response are associated with WISP1 expression in PCa, we examined LIF/LIFR, WISP1, and immune suppressive marker (suppressor of cytokine signaling 3 (SOCS3) and programmed death ligand 1 (PDL1)) expressions in various PCa cell lines. We found that 22Rv1, PC3, and LASCPC-01 cells had higher expressions of LIF, LIFR, WISP1, and immune suppressive markers, compared to LNCaP and C4-2 cells (Figure 3A). Immune suppressive cytokine stimulation was shown to be associated with an activated immune checkpoint pathway.[23] We demonstrated that the increased treatment of LNCaP and C4-2 cells with LIF protein could enhance the levels of WISP1, p-STAT3, PDL1, and SOCS3 proteins (Figures 3B and S3A). We also observed that LNCaP cells treated with the LIF protein had increased mRNA levels of *WISP1*, neuroendocrine markers, and stem cell markers, which were associated with *SOCS3* and *PDL1* mRNA abundances, whereas LIF-treated cells following LIF inhibitor (EC330) treatment had reduced mRNA expressions of these markers (Figure 3C). Furthermore, we demonstrated that in LNCaP and C4-2 cells, an increase in LIF protein levels led to the upregulation of WISP1 and p-STAT3 proteins, which were associated with increased abundances of SOCS3 and PDL1 proteins; however, this effect was abolished by treatment with a LIF inhibitor (Figure 3D). Moreover, we examined relative mRNA expression levels of *WISP1*, neuroendocrine markers, stem cell markers, anti-inflammatory markers, *LIF*, *CXCR2*, and *CXCL5* in LNCaP and C4-2 cells treated with the LIF recombinant protein, followed by *WISP1* siRNA expression. Results showed that cells treated with the LIF protein exhibited increased expressions of these markers and displayed a more neuroendocrine morphology compared to untreated cells, whereas cells expressing *WISP1*-knockdown (KD) showed a reduction in the effects of LIF (Figures 3E, S3B, and S3C). To study the functional roles of LIF/LIFR-driven WISP1 in PCa, LNCaP, and C4-2 cells were treated with the LIF protein, and WISP1 was further inhibited by expressing *WISP1* siRNA. Results showed that LIF-treated cells had increased cell proliferation and sphere formation, whereas silencing WISP1 reduced these effects regardless of LIF protein treatment (Figures 3F, 3G, S3D, and S3E). Moreover, LIF-treated cells showed increased cell migration and invasion through Matrigel, whereas
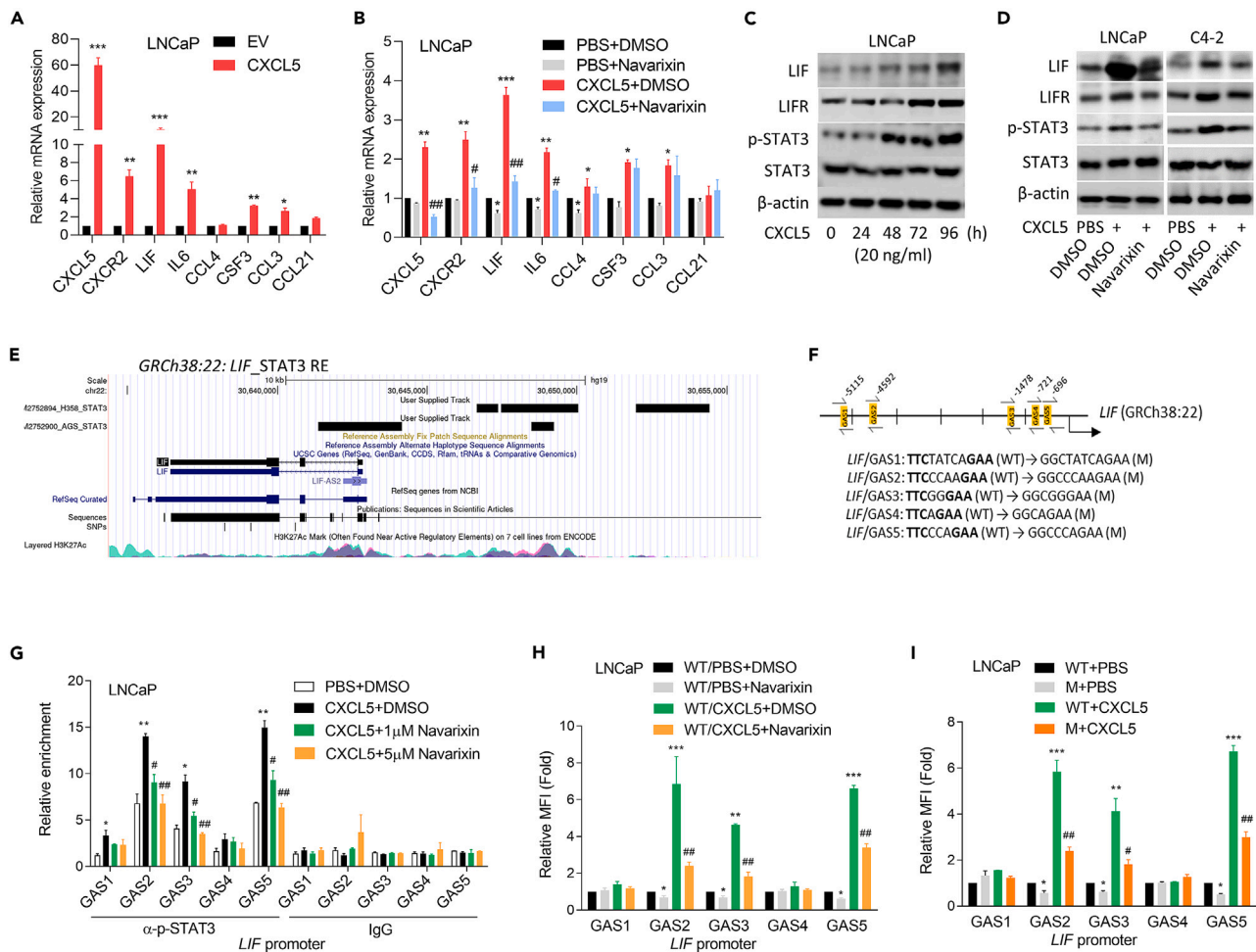
Figure 2. CXCL5/CXCR2 promotes LIF/LIFR/STAT3 signaling through the activation of the gamma interferon activation site (GAS) elements

(A) Relative mRNA levels of *CXCL5, CXCR2, LIF, IL6, CCL4, CSF3, CCL3,* and *CCL21* were measured in LNCaP cells stably transfected with an empty vector (EV) or a CXCL5-expressing vector. * vs. EV, as determined by a one-way ANOVA.

(B) Relative mRNA levels of *CXCL5, CXCR2, LIF, IL6, CCL4, CSF3, CCL3,* and *CCL21* were measured in LNCaP cells treated with PBS or 20 ng/mL of the CXCL5 recombinant protein, followed by treatment with DMSO or 5 μM navarixin for 48 h * vs. PBS+DMSO; # vs. CXCL5+DMSO, as determined by a one-way ANOVA.

(C) Relative protein levels of LIF, LIFR, phosphorylated (p)-STAT3, and STAT3 were measured in LNCaP cells treated with 20 ng/mL of the CXCL5 recombinant protein for 0 to 96 h.

(D) Relative protein levels of LIF, LIFR, p-STAT3, and STAT3 were measured in LNCaP and C4-2 cells treated with PBS or 20 ng/mL of CXCL5, followed by DMSO or 5 μM navarixin treatment for 48 h.

(E) ChIP-sequencing analysis revealed that p-STAT3 may bind to the GAS elements of the *LIF* gene, which is labeled as black boxes in the tracks. ChIP-sequencing data were downloaded from Gene Expression Omnibus (GEO) (GSM2752894) and analyzed by Genome Browser (Genomics Institute, UCSC).

(F) Schematic of the wild-type (WT) GAS and an introduced binding site mutant (M) in regulatory sequence reporter constructs of human *LIF* (GRCh38:22).

(G) The ChIP assay revealed the binding of p-STAT3 to the predicted GAS of the *LIF* gene regulatory sequence in LNCaP cells. Cells were treated with PBS or 20 ng/mL of CXCL5 recombinant protein and subsequently treated with DMSO or with either 1 μM or 5 μM navarixin for 48 h. Sheared chromatin from nuclear extracts was precipitated with antibodies against the p-STAT3 protein or control IgG, and we used predictive primers (F, black arrows) to quantify the precipitated DNA by qPCR. Enrichment of each protein to each site is given as a percentage of the total input and then normalized to IgG. * vs. PBS+DMSO; # vs. CXCL5+DMSO, as determined by a two-way ANOVA.

(H) The relative mean fluorescence intensity (MFI) of the GFP reporter gene, containing the WT-GAS from the *LIF* regulatory sequence, was measured in LNCaP cells. This measurement was taken after treatment with PBS or 20 ng/mL of the CXCL5 recombinant protein or combined treatment with DMSO or 5 μM navarixin for 48 h * vs. WT+PBS+DMSO; # vs. WT + CXCL5+DMSO, as determined by a one-way ANOVA.

(I) The relative MFI of the *GFP* reporter gene, containing the WT-GAS or M-GAS from the *LIF* regulatory sequence, was measured in LNCaP cells after 48 h of treatment with PBS or 20 ng/mL of the CXCL5 recombinant protein. * vs. WT + PBS; # vs. WT + CXCL5, as determined by a one-way ANOVA. Quantification of relative mRNA levels, p-STAT3 enrichment, and MFI is presented as the mean ± SEM from three biological replicates. *$p < 0.05$, **$p < 0.01$, ***$p < 0.005$.
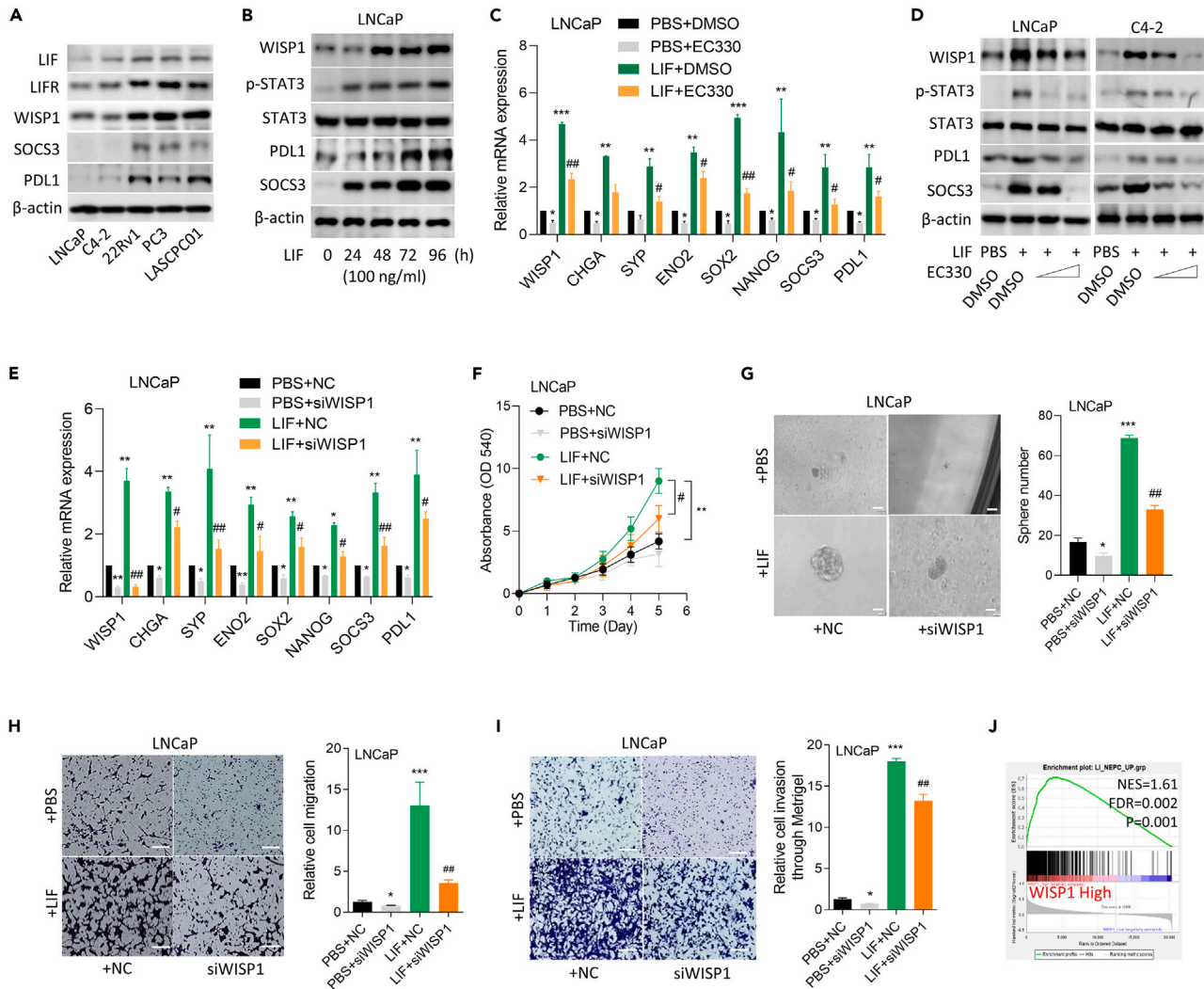
Figure 3. Knockdown of WPMY-1 suppresses LIF-driven neuroendocrine differentiation (NED) and malignant progression in prostate cancer (PCa) cells

(A) Relative protein levels of LIF, LIFR, WISP1, SOCS3, and PDL1 were measured in AR-positive PCa cell lines (LNCaP, C4-2, and 22Rv1), an AR-negative PCa cell line (PC3), and an NEPC cell line (LASCPC-01).

(B) Relative protein levels of WISP1, phosphorylated (p)-STAT3, STAT3, PDL1, and SOCS3 were measured in LNCaP cells treated with PBS or 100 ng/mL of the LIF recombinant protein for a duration ranging 0 to 96 h.

(C) Relative mRNA levels of *WISP1*, neuroendocrine (*CHGA*, *SYP*, and *ENO2*), stem cell (*SOX2* and *NANOG*), and anti-inflammatory (*SOCS3* and *PDL1*) markers in LNCaP cells treated with PBS or 100 ng/mL of the LIF recombinant protein or combined treatment with DMSO or 35 nM EC330 for 48 h * vs. PBS+DMSO; # vs. LIF+DMSO, as determined by a one-way ANOVA.

(D) Relative protein levels of WISP1, p-STAT3, STAT3, PDL1, and SOCS3 in LNCaP and C4-2 cells cultured in PBS or 100 ng/mL of the LIF recombinant protein, followed by DMSO or 35 nM EC330 treatment for 48 h.

(E) Relative mRNA expression levels of *WISP1*, neuroendocrine markers, stem cell markers, and anti-inflammatory markers (*SOCS3* and *PDL1*) were measured in LNCaP cells expressing the non-target control (NC) or *WISP1* siRNA, followed by treatment with PBS or 100 ng/mL of the LIF recombinant protein for 48 h * vs. PBS+NC; # vs. LIF+NC, as determined by a one-way ANOVA.

(F and G) Relative cell proliferation (F) and sphere formation (G) were measured in LNCaP cells expressing either NC or WISP1 siRNA, followed by treatment with either PBS or 100 ng/mL of LIF recombinant protein for 5 days (F) or 1 week (G). Scale bars represent 100 μm (G). * vs. PBS+NC; # vs. LIF+NC, as determined by a one-way ANOVA. (H and I) Relative cell migration (H) and invasion through Matrigel (I) were measured in LNCaP cells expressing the NC or WISP1 siRNA, followed by treatment with PBS or 100 ng/mL of LIF recombinant protein for 12 h. Scale bars representing 20 μm are shown. * vs. PBS+NC; # vs. LIF+NC, as determined by a one-way ANOVA. Quantification of relative mRNA levels, cell proliferation, sphere formation, and cell invasion through Matrigel is presented as the mean ± SEM from three biological replicates. *$p < 0.05$, **$p < 0.01$, ***$p < 0.005$.

(J) A GSEA of the TCGA PCa dataset revealed significant associations between high WISP1 expression in prostate tissues and a gene signature representing NEPC-responsive signaling. NES, normalized enrichment score; FDR, false discovery rate.

WISP1-KD abolished these effects (Figures 3H, 3I, S3F, and S3G). In addition, we conducted LIF inhibition and *WISP1*-KD experiments in the NEPC cell line LASCPC-01 to evaluate the impact of LIF or WISP1 on the mRNA expression of neuroendocrine markers, stem cell markers, *SOCS3, PDL1, LIF*, and *CXCL5*. Our findings revealed that inhibiting LIF or knocking down *WISP1* significantly reduced the expression of these markers in the LASCPC-01 NEPC cell line (Figures S4A and S4B). Furthermore, a GSEA of the TCGA prostate dataset revealed a significant association between high *WISP1* expression in prostate tissue and gene signatures representing CXCR2-dependent NEPC-responsive signaling (Figure 3J). Taken together, these results suggested that LIF-induced WISP1 may enhance cell malignancy in PCa, as it is associated with NED progression and immunosuppressive responses the PCa TME.

Activation of leukemia inhibitory factor/leukemia inhibitory factor receptor signaling in prostate cancer-stroma crosstalk promotes neuroendocrine differentiation and immunosuppressive cytokine expressions

Crosstalk between PCa cells and prostate stromal cells was investigated to understand its role in promoting NED and expressions of immunosuppressive cytokines within the TME through the activation of LIF/LIFR signaling. Relative mRNA expression levels of various markers were analyzed in LNCaP cells cultured with different concentrations of conditioned medium (CM) collected from human WPMY-1 stromal cells. Results showed that expression levels of *WISP1*, neuroendocrine markers (chromogranin A (*CHGA*), synaptophysin (*SYP*), and *ENO2*), stem cell markers (SRY box 2 (*SOX2*) and *NANOG*), and anti-inflammatory markers (*SOCS3* and *PDL1*) were significantly stimulated by increasing CM concentration (Figure 4A). Next, LNCaP cells were cultured with CM obtained from WPMY-1 stromal cells treated with the LIF inhibitor EC330. We observed that expression levels of *WISP1*, neuroendocrine markers, stem cell markers, and anti-inflammatory markers were decreased in cells treated with WPMY-1 CM in the presence of the LIF inhibitor (Figure 4B), highlighting the critical role of LIF/LIFR signaling in regulating these molecular changes. To further investigate the role of LIF/LIFR signaling in this crosstalk, we assessed relative mRNA expression levels of *WISP1*, neuroendocrine markers, stem cell markers, and anti-inflammatory markers in LNCaP cells cultured with CM collected from WPMY-1 cells expressing a non-target control (Luc) or *LIFR* shRNA. We observed significant increases in expressions of these markers in LNCaP cells treated with WPMY-1 CM compared to the vehicle group (Figure 4C). However, expressions of these markers were reduced when LNCaP cells were cultured with CM collected from *LIFR*-KD cells (Figure 4C). Furthermore, we examined mRNA expression levels of *LIFR, LIF*, immunosuppressive cytokines (*IL10, IL4*, IL-1 receptor antagonist (*IL1RN*), transforming growth factor β1 (*TGFB1*), interferon-α17 (*IFNA17*), and *SOCS3*), *CXCL5, WISP1*, and vascular endothelial growth factor A (*VEGFA*) in WPMY-1 cells expressing shLuc or *LIFR* shRNA. We observed significant decreases in the expression of these markers in WPMY-1 cells expressing *LIFR*-KD compared to the control cells (Figure 4D). WPMY-1 cells treated with the LIF recombinant protein exhibited increased expressions of these markers; however, when treated with a combination of the LIF recombinant protein and an LIF inhibitor, expression levels of these markers were reduced (Figure 4E). To assess the functional implications of this crosstalk, we evaluated cell proliferation and sphere formation in LNCaP cells cultured with CM obtained from WPMY-1 stromal cells. Results revealed significant increases in cell proliferation and sphere formation in LNCaP cells treated with WPMY-1 CM compared to the control group (Figures 4F and 4G). However, these effects were eliminated when cells were cultured with CM obtained from WPMY-1 stromal cells treated with an LIF inhibitor (Figures 4F and 4G). We investigated the effects of crosstalk on cell migration and invasion through Matrigel. We observed significant increases in cell migration and invasion through Matrigel in LNCaP cells cultured with CM obtained from WPMY-1 stromal cells; however, these effects decreased when cells were cultured with CM obtained from WPMY-1 stromal cells treated with an LIF inhibitor (Figures 4H and 4I). These findings highlight the significant impact of LIF/LIFR signaling on the crosstalk between PCa cells and prostate stromal cells in promoting NED and modulating immunosuppressive cytokines within the PCa TME.

Leukemia inhibitory factor/signal transducer and activator of transcription 3-mediated transcription of the WNT1-inducible signaling pathway protein 1 and leukemia inhibitory factor genes through direct binding to gamma interferon activation site elements in the regulatory sequence

We investigated the regulatory mechanism underlying the transcriptional activation of *WISP1* by LIF/STAT3 signaling through direct binding to GAS elements in the regulatory sequence. A ChIP-sequencing analysis was conducted using ChIP-sequencing data obtained from GEO (GSM2752894 and GSM2752900), and data were analyzed using the Genome Browser (Genomics Institute) to identify GAS elements for *WISP1*. The analysis revealed specific GAS elements, which are depicted as black boxes in tracks (Figure 5A). WISP1 abundance was observed in prostate stromal cells and was correlated with tumor progression.[17,19,20] Using the PROMO database of transcription factor-binding profiles,[21] we conducted a search for sequences resembling GAS elements in the regulatory sequence of *WISP1*. Our analysis identified one putative GAS element upstream and two downstream of the *WISP1* transcription start site (Figure 5B). ChIP assays were conducted in LNCaP cells and prostate stromal WPMY-1 cells to validate the direct binding of p-STAT3 to the predicted GASs in the *WISP1* gene regulatory sequence. These cells were treated with the LIF recombinant protein, followed by treatment with the LIF inhibitor EC330. Chromatin from nuclear extracts was immunoprecipitated with antibodies to p-STAT3 or IgG, and a qPCR was performed using predictive primers to quantify precipitated DNA. Results demonstrated the binding of p-STAT3 to GAS1 and GAS3 of the *WISP1* gene regulatory sequence in LNCaP cells and WPMY-1 cells (Figures 5C and 5D). Furthermore, ChIP assays were performed to investigate the binding of p-STAT3 to predicted GASs in the regulatory sequence of the *LIF* gene in WPMY-1 cells. Cells were treated with the LIF recombinant protein, followed by treatment with various LIF inhibitor concentrations. Results confirmed the binding of p-STAT3 to GAS2, GAS3, and GAS5 in the *LIF* gene regulatory sequence (Figure 5E). To evaluate the functional significance of GASs in the *WISP1* regulatory sequence, relative mean florescence intensity (MFI) of the GFP reporter gene containing the WT-GAS or M-GAS were measured in LNCaP and WPMY-1 cells. Cells were treated with the LIF
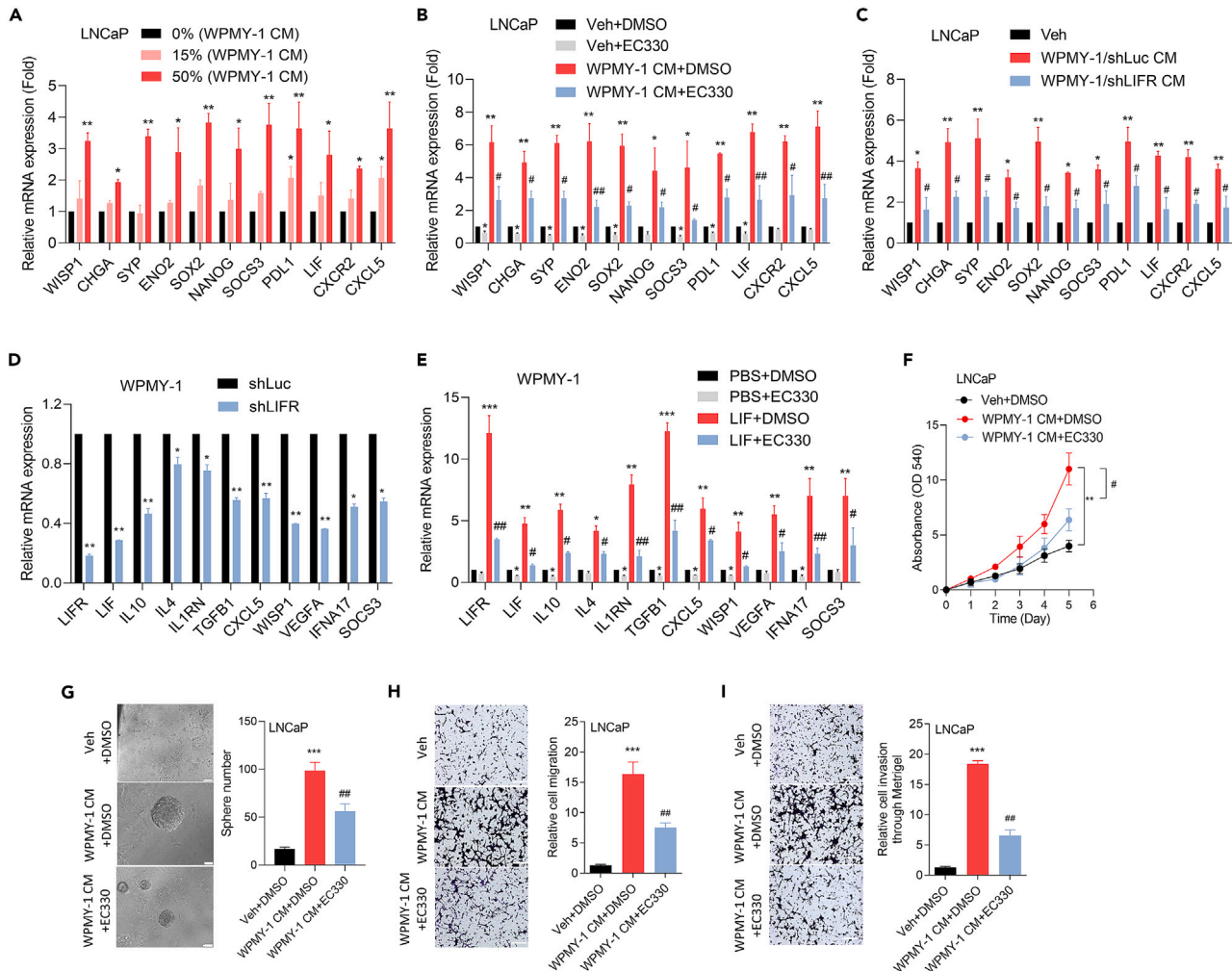
Figure 4. Crosstalk between prostate cancer (PCa) cells and prostate stromal cells promotes neuroendocrine differentiation (NED) and expressions of immunosuppressive cytokines in the tumor microenvironment (TME) through the activation of LIF/LIFR signaling

(A) Relative mRNA expression levels of *WISP1*, neuroendocrine markers (*CHGA*, *SYP*, and *ENO2*), stem cell markers (*SOX2* and *NANOG*), anti-inflammatory markers (*SOCS3* and *PDL1*), *LIF*, *CXCR2*, and *CXCL5* in LNCaP cells. These cells were cultured with conditioned medium (CM) collected from human WPMY-1 stromal cells, at concentrations of 0%, 15%, or 50%, for a duration of 48 h * vs. 0%, as determined by a one-way ANOVA.

(B) Relative mRNA expression levels of *WISP1*, neuroendocrine markers, stem cell markers, anti-inflammatory markers, *LIF*, *CXCR2*, and *CXCL5* were measured in LNCaP cells. These cells were cultured with CM obtained from WPMY-1 stromal cells treated with DMSO or 35 nM EC330 for 48 h * vs. Veh+DMSO; # vs. WPMY-1 CM + DMSO, as determined by a one-way ANOVA.

(C) Relative mRNA expression levels of *WISP1*, neuroendocrine, stem cell, anti-inflammatory markers, *LIF*, *CXCR2*, and *CXCL5* in LNCaP cells cultured with CM collected from the non-target control (Luc) or *LIFR* shRNA-expressing WPMY-1 cells for 48 h * vs. Veh; # vs. WPMY-1/shLuc CM, as determined by a one-way ANOVA.

(D) Relative mRNA expression levels of *LIFR*, *LIF*, *CXCL5*, *WISP1*, and anti-inflammatory markers (*IL10*, *IL4*, *IL1RN*, *TGFB1*, *VEGFA*, *IFNA17*, and *SOCS3*) in WPMY-1 cells stably expressing the shLuc or *LIFR* shRNA. * vs. shLuc, as determined by a one-way ANOVA.

(E) Relative mRNA expression levels of *LIFR*, *LIF*, *CXCL5*, *WISP1*, and anti-inflammatory markers in WPMY-1 cells treated with PBS or 100 ng/mL of the LIF recombinant protein, followed by DMSO or 35 nM EC330 treatment for 48 h * vs. PBS+DMSO; # vs. LIF+DMSO, as determined by a one-way ANOVA.

(F and G) Cell proliferation (F) and sphere formation (G) of LNCaP cells were evaluated. These cells were cultured with CM obtained from WPMY-1 stromal cells treated with DMOS or 35 nM EC330 for 48 h. Scale bars in (G) represent 100 μm. Statistical comparisons were performed using a one-way ANOVA. * vs. Veh+DMSO; # vs. WPMY-1 CM + DMSO.

(H and I) Relative cell migration (H) and invasion through Matrigel (I) were measured in LNCaP cells. These cells were cultured with CM obtained from WPMY-1 stromal cells treated with DMSO or 35 nM EC330 for 12 h. Scale bars representing 20 μm are shown. * vs. Veh+DMSO; # vs. WPMY-1 CM + DMSO, as determined by a one-way ANOVA. Quantification of relative mRNA levels, cell proliferation, sphere formation, and cell invasion through Matrigel is presented as the mean ± SEM, based on three biological replicates. Significance levels are denoted as *$p < 0.05$, **$p < 0.01$, and ***$p < 0.005$.
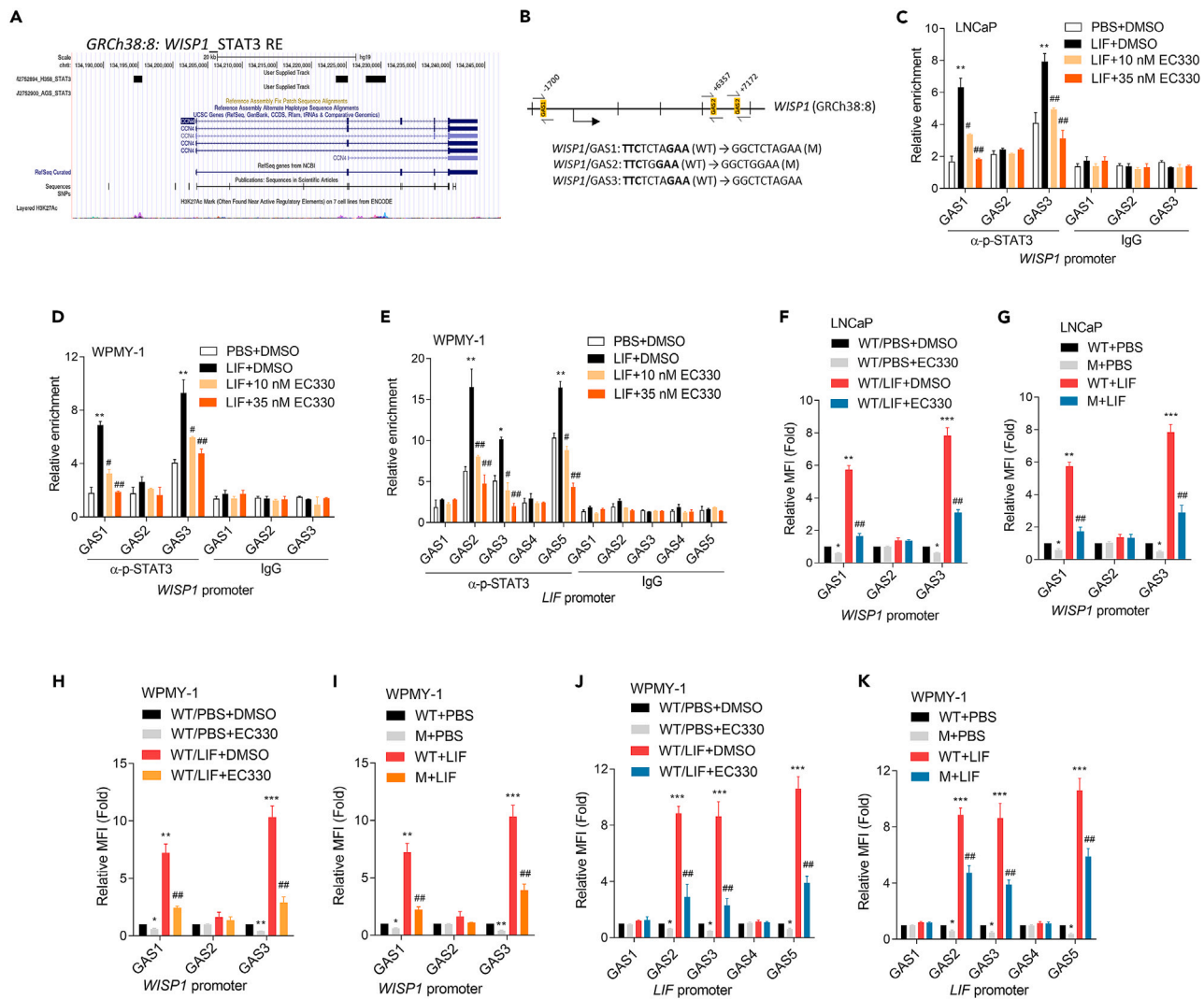
Figure 5. LIF/STAT3-driven transcription of *WISP1* through direct binding to the gamma interferon activation site (GAS) of the regulatory sequence

(A) ChIP-sequencing analysis was performed to detect the GAS for *WISP1*. Detected GAS sites are labeled as black boxes in the tracks. ChIP-sequencing data were downloaded from Gene Expression Omnibus (GEO) (GSM2752900) and analyzed using the Genome Browser (Genomics Institute, UCSC).

(B) A schematic representation is shown for the predicted wild-type (WT) and mutant (M)-GASs in the regulatory sequence reporter constructs of the human *WISP1* gene (GRCh38:8) (C and D) A ChIP assay was performed to show the binding of phosphorylated (p)-STAT3 to the predicted GAS in the *WISP1* gene regulatory sequence. The assay was conducted in LNCaP cells (C) or WPMY-1 cells (D) treated with PBS or 100 ng/mL of the LIF recombinant protein, followed by treatment with DMSO or with 10 or 35 nM EC330 for 48 h. Sheared chromatin from nuclear extracts was precipitated with antibodies to p-STAT3 or control IgG, and predictive primers (B, indicated by black arrows) were used to quantify the precipitated DNA using a qPCR. Enrichment of each protein at each site is presented as a percentage of the total input and then normalized to IgG. * vs. PBS+DMSO; # vs. LIF+DMSO, as determined by a one-way ANOVA.

(E) A ChIP assay was performed to demonstrate the binding of p-STAT3 to the predicted GAS in the regulatory sequence of the *LIF* gene in WPMY-1 cells. Cells were treated with PBS or 100 ng/mL of the LIF recombinant protein, followed by treatment with DMSO or with 10 or 35 nM EC330 for 48 h * vs. PBS+DMSO; # vs. LIF+DMSO, as determined by a one-way ANOVA.

(F–I) The relative mean fluorescence intensity (MFI) of the GFP reporter gene containing either the WT-GAS or M-GAS from the *WISP1* regulatory sequence was measured in LNCaP cells (F and G) and WPMY-1 cells (H and I) after treatment with PBS or 100 ng/mL of LIF recombinant protein. This was followed by further treatment with either DMSO or EC330 (10 or 35 nM) for 48 h (F and H). * vs. WT/PBS+DMSO (F and H) or WT + PBS (G and I); # vs. WT/LIF+DMSO (F and H) or WT + LIF (G and I), as determined by a one-way ANOVA.

(J and K) The relative MFI of the GFP reporter gene containing the WT-GAS or M-GAS from the *LIF* regulatory sequence was measured in WPMY-1 cells treated with PBS or 100 ng/mL of LIF recombinant protein or combined treatment with DMSO or 10 or 35 nM EC330 for 48 h * vs. WT/PBS+DMSO (J) or WT + PBS (K); # vs. WT/LIF+DMSO (J) or WT + LIF (K), as determined by a one-way ANOVA. Quantification of relative p-STAT3 enrichment and MFI is presented as the mean ± SEM from three biological replicates. *$p < 0.05$, **$p < 0.01$, ***$p < 0.005$.

recombinant protein or combined with an LIF inhibitor. The MFI of the *WISP1*-GFP reporter gene containing the WT-GAS was compared to the vehicle or LIF treatment, while the MFI of the *WISP1*-GFP reporter gene containing the M-GAS was compared to the WT-GAS plus LIF treatment. Results revealed that the LIF recombinant protein significantly increased WT-GAS-containing *WISP1*-GFP reporter activity in both LNCaP and WPMY-1 cells compared to the vehicle, and this effect was attenuated by EC330 treatment (Figures 5F and 5H). Moreover, the M-GAS did not produce a significant increase in *WISP1*-GFP reporter activity upon LIF treatment (Figures 5G and 5I). In addition, the relative MFI of the GFP reporter gene containing the WT or M-GAS from the *LIF* regulatory sequence was measured in WPMY-1 cells treated with the LIF recombinant protein or combined with an LIF inhibitor. We found that the LIF treatment of WPMY-1 cells significantly enhanced the activity of the *LIF*-GFP reporter containing the WT-GAS sequence compared to the vehicle; however, this effect was diminished by EC330 treatment or when the *LIF*-GFP reporter gene containing the M-GAS sequence was present (Figures 5J and 5K). Taken together, our findings suggested that LIF/STAT3 signaling drives the transcriptional activation of *WISP1* and *LIF* by directly binding to the GAS in the regulatory sequence. This regulatory mechanism provides insights into the molecular basis of LIF-mediated *WISP1* and *LIF* expressions in PCa and prostate stromal cells.

WNT1-inducible signaling pathway protein 1 abundance in serum reflects prostate cancer progression

To demonstrate the importance of CXCL5/CXCR2/LIF/WISP1 in PCa NED, we used C4-2 cells overexpressing CXCL5 and treated them with the LIF inhibitor EC330. Results showed that cells with CXCL5 overexpression induced the mRNA expression of *CXCR2, LIF, WISP1,* neuroendocrine, and stem cell markers and displayed a more neuroendocrine morphology compared to control cells; however, treatment with the LIF inhibitor reduced these properties in CXCL5-overexpressing cells (Figures 6A and S4C). An *in vivo* experiment involved the subcutaneous injection of both empty vector (EV)-expressing cells and CXCR5-overexpressing cells, followed by the treatment of these mice with the LIF inhibitor via intravenous injection. The findings indicated an increase in tumor growth and tumor weights in CXCL5-overexpressing cells, whereas a decrease in both tumor growth and tumor weights was observed in these mice when treated with the LIF inhibitor (Figures 6B and 6C). Further analysis of harvested tumors through immunohistochemistry (IHC) staining revealed that CXCL5 overexpression elevated CXCR2, LIF, WISP1, and neuroendocrine marker levels, which were diminished with EC330 treatment (Figures 6D and 6E). Next, we examined the abundance of WISP1 in patient sera relative to PCa progression. Patient sera were collected from individuals with benign prostatic hyperplasia (BPH), hormone-sensitive PCa (HSPC), and metastatic CRPC (mCRPC). WISP1 concentrations in sera were measured, and comparisons were made among the different groups. The results showed significantly higher concentrations of WISP1 in mCRPC samples compared to HSPC and higher concentrations of WISP1 in mCRPC samples compared to BPH samples (Figure 6F). These findings suggest the potential of WISP1 to be a biomarker for metastatic CRPC progression. A recent study profiled the immunogenomic landscape of NEPC and concluded that NEPC has a relatively immunosuppressive TME.[24] The LIF is involved in regulating T cell responses, including the suppression of tumor-infiltrating CD8$^+$ T cell function.[25] To investigate the association between LIF abundance and WISP1 expression in patients with PCa, we conducted a series of analyses using publicly available datasets and computational tools. First, we performed a GSEA on the TCGA prostate dataset to identify potential associations between high LIF and WISP1 expressions in prostate tissues. GSEAs results revealed significant associations of high LIF levels and WISP1 expression and gene signatures representing metastatic prostatic stroma (Figure 6G), IL-10-responsive signaling, and transforming growth factor β (TGF-β)-responsive signaling (Figure S5A). Next, we employed Spearman's correlation analyses to explore relationships of LIF or WISP1 expressions and infiltrating immune cells associated with inflammation in PCa. Using the TIMER2 database,[26] we found positive correlations of LIF and WISP1 expressions with various anti-inflammatory infiltrating cells, including CAFs, regulatory T (Treg) cells, and M2 macrophages (Figure S5B). Conversely, Spearman's correlation analyses revealed negative relationships of LIF and WISP1 expressions and proinflammatory infiltrating cells, such as CD4$^+$ T cells, CD8$^+$ T cells, and B cells (Figure S5C). Taken together, our results indicated that LIF abundance in patients with PCa was associated with increased WISP1 expression. Furthermore, we observed positive correlations of LIF and WISP1 expressions with anti-inflammatory infiltrating cells, while negative correlations were observed with proinflammatory infiltrating cells. These findings suggest potential roles for LIF and WISP1 in modulating the immune microenvironment in PCa, favoring an anti-inflammatory response while suppressing proinflammatory signaling. In summary, our findings suggested that there is crosstalk between PCa cells and prostate stromal cells within the TME. This crosstalk potentially enhances interactions between CXCL5/CXCR2 and the LIF/LIFR pathway. The interaction between these pathways may lead to the upregulation of the LIF and WISP1 proteins. This upregulation is facilitated by the critical roles of p-STAT3/GAS signaling-driven activation of the *WISP1* and *LIF* genes. Crosstalk between PCa and prostate stromal cells may enhance the LIF/LIFR signaling-driven immunosuppressive TME and NED in PCa cells through the upregulation of the *WISP1* and *LIF* genes (Figure 6H).

DISCUSSION

Our research findings provide compelling evidence supporting the existence of intricate interplay between CXCL5/CXCR2 signaling and the expression of an LIF-driven immunosuppressive response in the PCa TME. We discovered that the interaction between CXCL5/CXCR2 and LIF/LIFR signaling leads to the phosphorylation of STAT3, suggesting the presence of a potential feedback loop between these pathways within the PCa TME. CXCR2, a member of the GPCR family, acts as a high-affinity receptor for IL-8 and other ligands, including CXCL5.[27] CXCL5, expressed and secreted in an autocrine manner by tumor cells, promotes synergistic effects on endothelial cell proliferation.[28] Activation of CXCL5/CXCR2 stimulates the JAK2/STAT3 axis, driving angiogenic responses in tumors through the CXCR2/AKT/nuclear factor (NF)-κB/forkhead box D1 (FOXD1)/VEGFA signaling pathway.[28] Conversely, the activation of STAT3 also increases CXCR2 expression, which then activates STAT3 through the activation of the Raf-MAPK kinase (MEK)-extracellular signal-regulated kinase (ERK) pathway, suggesting a
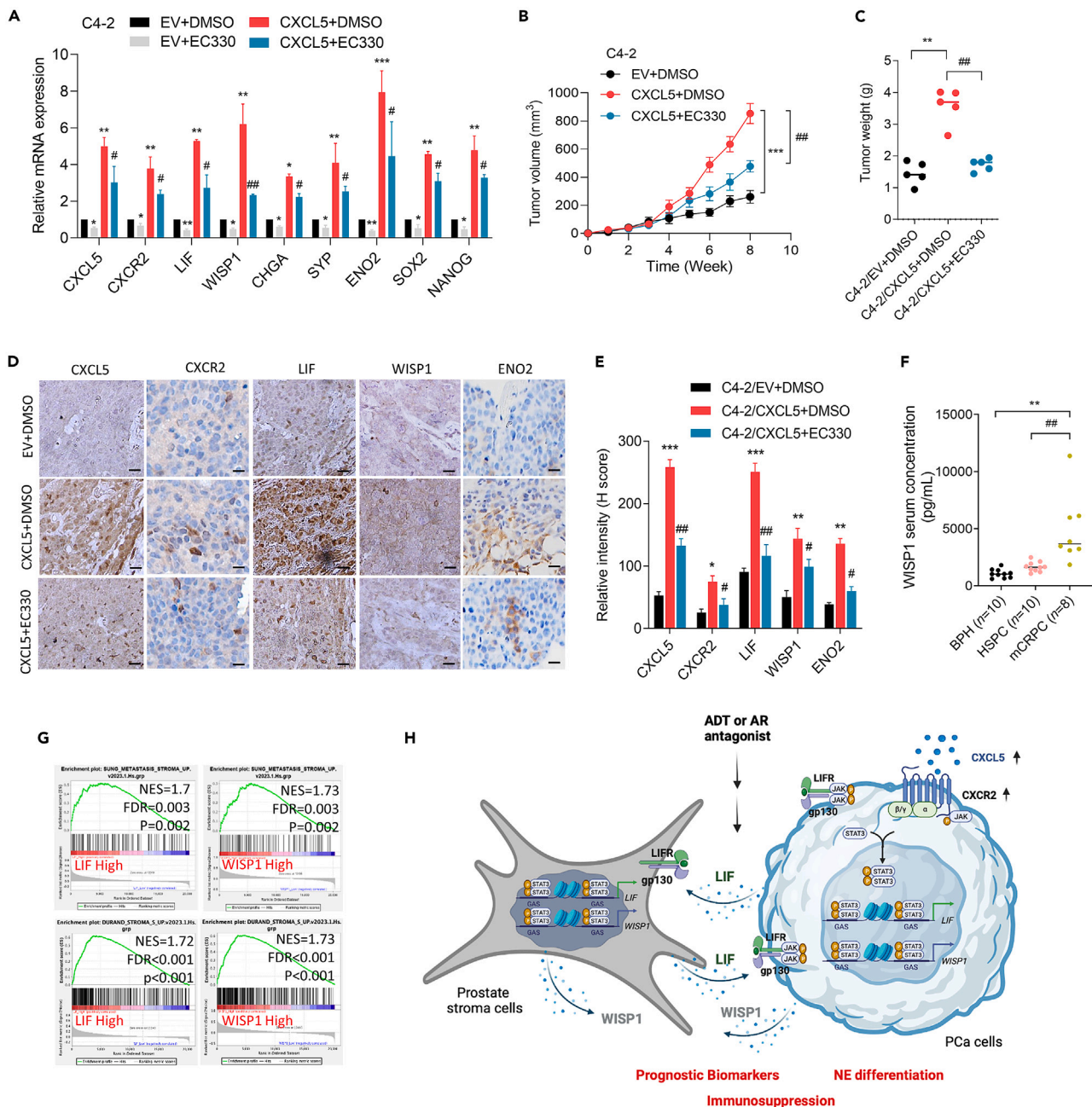
Figure 6. WISP1 abundance in serum relative to prostate cancer (PCa) progression

(A) Relative mRNA levels of *CXCL5, CXCR2, LIF, WISP1,* neuroendocrine (*CHGA, SYP,* and *ENO2*), and stem cell (*SOX2* and *NANOG*) markers in C4-2 cells expressing the empty vector (EV) or CXCL5-expressing vector, followed by treatment with DMSO or 35 nM EC330 for 48 h * vs. EV + DMSO; # vs. CXCL5+DMSO, as determined by a one-way ANOVA.

(B and C) Tumor growth analysis was conducted by subcutaneously inoculating male nude mice with C4-2 cells expressing either the EV or a CXCL5-expressing vector. The mice were then treated bi-daily with either DMSO or 2.5 mg/kg EC330 via intraperitoneal injection and allowed to grow for 8 weeks. Tumor sizes were measured weekly (B). Tumor weights were measured upon tumor collection (C). *n* = 5 per group. * vs. EV + DMSO; # vs. CXCL5+DMSO, as determined by a one-way ANOVA and t-test.

(D and E) Immunohistochemical (IHC) staining and intensity analyses were performed to assess protein levels of CXCL5, CXCR2, LIF, WISP1, and ENO2 in subcutaneous tumors derived from (B). * vs. EV + DMSO; # vs. CXCL5+DMSO, as determined by a two-tailed Student's t-test. Scale bars, 100 μm.

(F) WISP1 concentrations were measured in patient sera derived from samples of benign prostatic hyperplasia (BPH; *n* = 10), hormone-sensitive PCa (HSPC, *n* = 10), and metastatic castration-resistant PCa (mCRPC; *n* = 8). * vs. BPH; # vs. HSPC, analyzed by a one-way ANOVA.

Figure 6. Continued

(G) GSEAs of the TCGA PCa dataset revealed significant associations between high LIF and WISP1 expressions in prostate tissues with gene signatures representing metastatic prostate stroma-responsive signaling. NES, normalized enrichment score; FDR, false discovery rate.

(H) A schematic summary of this study is presented. Crosstalk between PCa cells and prostate stromal cells within the tumor microenvironment (TME) may enhance the interaction between the CXCL5/CXCR2 and LIF/LIFR pathways. This interaction can potentially upregulate the secretion of LIF and WISP1 proteins, facilitated by the critical roles of STAT3 signaling-driven activation of the *WISP1* and *LIF* genes.

feedforward loop interaction between STAT3 and CXCR2.[9] Additionally, CXCL5 binding to CXCR2 may increase JAK2 phosphorylation, inducing STAT3 activation.[29] However, limited research has been conducted on the mechanisms of how CXCL5/CXCR2 activation in PCa after ADT or paracrine signaling between tumor cells and prostate stromal cells contributes to the immunosuppressive TME and NED in PCa.

In this study, we aimed to characterize the molecular mechanisms underlying the immunosuppressive response and their impacts on NED in PCa. We also sought to investigate correlations between abundances of immunosuppressive cytokines and the malignant progression of PCa after ADT. Our results identified crosstalk between CXCL5/CXCR2 and LIF/LIFR, leading to the activation of a STAT3-driven transcription network and the potential upregulation of WISP1. However, it remains unclear whether PCa cells, after developing resistance to ADT, express WISP1 in the TME through interactions with prostate stromal cells, ultimately contributing to an LIF/LIFR-driven anti-inflammatory phenotype or NED progression. Our findings suggested that the stimulation of the LIF immunomodulatory cytokine may induce interactions with PCa stromal cells, activating p-STAT3-driven WISP1 expression in the PCa TME, thereby enhancing immunosuppressive responses and promoting NEPC development.

STAT3 can be phosphorylated by various factors, including growth factors, cytokines, interferons, and oncogenes.[30] STAT3 was found to be phosphorylated in various cancers and to drive gene expression from GAS-containing promoters to enhance tumorigenesis.[31] In PCa, p-STAT3 forms dimers and is translocated to nuclei, where it activates the transcription of target genes.[32] We demonstrated that LIF/LIFR induces the phosphorylation of STAT3, leading to the transcriptional activation of *WISP1* through direct binding to the GAS in the regulatory sequence. Increased WISP1 expression was associated with tumor progression in various cancer types, including PCa.[17] However, the role of WISP1 in the development of NEPC remains unclear. Our results suggested that the activation of LIF/LIFR signaling may upregulate WISP1 expression, promoting the carcinogenesis of PCa cells. Furthermore, we revealed that LIF can activate p-STAT3 to bind to the GAS elements of *WISP1* in both PCa cells and stromal cells, thereby promoting an immunosuppressive response and the malignant progression of PCa.

Notably, there is currently no effective clinical treatment strategy for NEPC or aggressive small-cell PCa (SCPC). Although NEPC and SCPC are characterized by expressions of neuroendocrine cell-specific genes and frequently harbor specific gene mutations, there is a lack of clinically effective cell surface biomarkers for their diagnosis.[33] If tumor-specific antigens expressed on the surface of NEPC tumor cells could be identified, targeted drugs could be developed, facilitating the use of immunotherapeutic combinations for treating neuroendocrine-like PCa. Our findings suggest that the upregulation of the LIF in both PCa cells and stromal cells may link NED to the immunosuppressive TME through the activation of the LIF/LIFR/STAT3 axis. Therefore, targeting the LIFR as a therapeutic approach for NEPC treatment could hold clinical significance, considering the distribution of the LIFR on the cell surfaces of PCa and immune cells.[14,34]

In summary, our study highlights the intricate interplay between CXCL5/CXCR2 signaling and the LIF-driven immunosuppressive response in the PCa TME. We discovered that the interaction between CXCL5/CXCR2 and LIF/LIFR signaling leads to STAT3 phosphorylation, suggesting the presence of a feedback loop between these pathways. We demonstrated that this crosstalk activates a STAT3-driven transcription network and potentially upregulates WISP1 expression. Moreover, our findings indicated that LIF/LIFR stimulation induces interactions between PCa cells and prostate stromal cells, promoting an immunosuppressive TME and contributing to the NED of PCa. The main motivation of our study was to shed light on the molecular mechanisms underlying NED and the immunosuppressive TME in PCa, particularly in the context of resistance to ADT. Ultimately, our study contributes to an understanding of PCa progression and may pave the way for potential therapeutic approaches, including immunotherapy and small-molecule targeted therapy, to improve patient outcomes.

Limitations of the study

While we identified key interactions and pathways, the precise molecular mechanisms through which CXCL5/CXCR2 activation contributes to NED and the immunosuppressive TME in PCa post-ADT remain unclear. Further research is needed to elucidate these processes in greater detail. The study suggests a potential upregulation of WISP1 in the TME; however, it is unclear if and how WISP1 expression dynamically changes in PCa cells that have developed resistance to ADT. Longitudinal studies are required to understand these dynamics better. Although our findings propose WISP1 as a potential biomarker and suggest targeting LIFR for NEPC treatment, the lack of clinically validated biomarkers and targeted therapies for NEPC and SCPC remains a significant challenge. Further clinical research is required to develop and validate these potential therapeutic targets.

STAR★METHODS

Detailed methods are provided in the online version of this paper and include the following:

- KEY RESOURCES TABLE
- RESOURCE AVAILABILITY
  - Lead contact

SUPPLEMENTAL INFORMATION

Supplemental information can be found online at https://doi.org/10.1016/j.isci.2024.110562.

AUTHOR CONTRIBUTIONS

Conceptualization, K.H.T. and Y.-N.L.; methodology, M.H., W.A.-K., and Y.-N.L.; data curation, H.-L.Y., M.-K.L.,W.-H.C., K.-C.J., H.-R.L., and Y.-N.L.; investigation, H.-L.Y., M.-K.L.,C.-H.L., W.-H.C., K.-C.J., H.-R.L., and P.V.T.D.; formal analysis, H.-L.Y., M.-K.L.,W.-H.C., K.-C.J., H.-R.L., and Y.-N.L.; validation, H.-L.Y., M.-K.L.,W.-H.C., K.-C.J., H.-R.L., and Y.-N.L.; resources, M.H. and Y.-N.L.; writing – original draft, Y.-N.L.; review and editing, W.A.-K. and Y.-N.L.; supervision, Y.-N.L.; project administration, Y.-N.L.; funding acquisition, K.H.T., C.-L.L., and Y.-N.L. All authors have read, edited, and approved the final article.

DECLARATION OF INTERESTS

The authors declare that there are no potential conflicts of interest.

REFERENCES

1. Litwin, M.S., and Tan, H.J. (2017). The Diagnosis and Treatment of Prostate Cancer: A Review. JAMA *317*, 2532–2542. https://doi.org/10.1001/jama.2017.7248.

2. Wang, Q., Li, W., Zhang, Y., Yuan, X., Xu, K., Yu, J., Chen, Z., Beroukhim, R., Wang, H., Lupien, M., et al. (2009). Androgen receptor regulates a distinct transcription program in androgen-independent prostate cancer. Cell *138*, 245–256. https://doi.org/10.1016/j.cell.2009.04.056.

3. Yamada, Y., and Beltran, H. (2021). Clinical and Biological Features of Neuroendocrine Prostate Cancer. Curr. Oncol. Rep. *23*, 15. https://doi.org/10.1007/s11912-020-01003-9.

4. Tzelepi, V., Zhang, J., Lu, J.F., Kleb, B., Wu, G., Wan, X., Hoang, A., Efstathiou, E., Sircar, K., Navone, N.M., et al. (2012). Modeling a lethal prostate cancer variant with small-cell carcinoma features. Clin. Cancer Res. *18*, 666–677. https://doi.org/10.1158/1078-0432.CCR-11-1867.

5. Li, Z., Zhou, J., Zhang, J., Li, S., Wang, H., and Du, J. (2019). Cancer-associated fibroblasts promote PD-L1 expression in mice cancer cells via secreting CXCL5. Int. J. Cancer *145*, 1946–1957. https://doi.org/10.1002/ijc.32278.

6. Di Mitri, D., Mirenda, M., Vasilevska, J., Calcinotto, A., Delaleu, N., Revandkar, A., Gil, V., Boysen, G., Losa, M., Mosole, S., et al. (2019). Re-education of Tumor-Associated Macrophages by CXCR2 Blockade Drives Senescence and Tumor Inhibition in Advanced Prostate Cancer. Cell Rep. *28*, 2156–2168.e5. https://doi.org/10.1016/j.celrep.2019.07.068.

7. Li, Y., He, Y., Butler, W., Xu, L., Chang, Y., Lei, K., Zhang, H., Zhou, Y., Gao, A.C., Zhang, Q., et al. (2019). Targeting cellular heterogeneity with CXCR2 blockade for the treatment of therapy-resistant prostate cancer. Sci. Transl. Med. *11*, eaax0428. https://doi.org/10.1126/scitranslmed.aax0428.

8. Romero-Moreno, R., Curtis, K.J., Coughlin, T.R., Miranda-Vergara, M.C., Dutta, S., Natarajan, A., Facchine, B.A., Jackson, K.M.,

Nystrom, L., Li, J., et al. (2019). The CXCL5/CXCR2 axis is sufficient to promote breast cancer colonization during bone metastasis. Nat. Commun. *10*, 4404. https://doi.org/10.1038/s41467-019-12108-6.

9. Nguyen-Jackson, H., Panopoulos, A.D., Zhang, H., Li, H.S., and Watowich, S.S. (2010). STAT3 controls the neutrophil migratory response to CXCR2 ligands by direct activation of G-CSF-induced CXCR2 expression and via modulation of CXCR2 signal transduction. Blood *115*, 3354–3363. https://doi.org/10.1182/blood-2009-08-240317.

10. Levesque, C., and Nelson, P.S. (2018). Cellular Constituents of the Prostate Stroma: Key Contributors to Prostate Cancer Progression and Therapy Resistance. Cold Spring Harb. Perspect. Med. *8*, a030510. https://doi.org/10.1101/cshperspect.a030510.

11. Quail, D.F., and Joyce, J.A. (2013). Microenvironmental regulation of tumor progression and metastasis. Nat. Med. *19*, 1423–1437. https://doi.org/10.1038/nm.3394.

12. Ge, D., Gao, A.C., Zhang, Q., Liu, S., Xue, Y., and You, Z. (2012). LNCaP prostate cancer cells with autocrine interleukin-6 expression are resistant to IL-6-induced neuroendocrine differentiation due to increased expression of suppressors of cytokine signaling. Prostate *72*, 1306–1316. https://doi.org/10.1002/pros.22479.

13. Liu, Y.N., Niu, S., Chen, W.Y., Zhang, Q., Tao, Y., Chen, W.H., Jiang, K.C., Chen, X., Shi, H., Liu, A., et al. (2019). Leukemia Inhibitory Factor Promotes Castration-resistant Prostate Cancer and Neuroendocrine Differentiation by Activated ZBTB46. Clin. Cancer Res. *25*, 4128–4140. https://doi.org/10.1158/1078-0432.CCR-18-3239.

14. Lin, S.R., Wen, Y.C., Yeh, H.L., Jiang, K.C., Chen, W.H., Mokgautsi, N., Huang, J., Chen, W.Y., and Liu, Y.N. (2020). EGFR-upregulated LIFR promotes SUCLG2-dependent castration resistance and neuroendocrine differentiation of prostate cancer. Oncogene *39*, 6757–6775. https://doi.org/10.1038/s41388-020-01468-9.

15. Deng, W., Fernandez, A., McLaughlin, S.L., and Klinke, D.J. (2019). WNT1-inducible signaling pathway protein 1 (WISP1/CCN4) stimulates melanoma invasion and metastasis by promoting the epithelial-mesenchymal transition. J. Biol. Chem. *294*, 5261–5280. https://doi.org/10.1074/jbc.RA118.006122.

16. Chang, K.S., Chen, S.T., Sung, H.C., Hsu, S.Y., Lin, W.Y., Hou, C.P., Lin, Y.H., Feng, T.H., Tsui, K.H., and Juang, H.H. (2022). WNT1 Inducible Signaling Pathway Protein 1 Is a Stroma-Specific Secreting Protein Inducing a Fibroblast Contraction and Carcinoma Cell Growth in the Human Prostate. Int. J. Mol. Sci. *23*, 11437. https://doi.org/10.3390/ijms231911437.

17. Gaudreau, P.O., Clairefond, S., Class, C.A., Boulay, P.L., Chrobak, P., Allard, B., Azzi, F., Pommey, S., Do, K.A., Saad, F., et al. (2019). WISP1 is associated with advanced disease, EMT and an inflamed tumor microenvironment in multiple solid tumors. OncoImmunology *8*, e1581545. https://doi.org/10.1080/2162402x.2019.1581545.

18. Fernandez, A., Deng, W., McLaughlin, S.L., Pirkey, A.C., Rellick, S.L., Razazan, A., and Klinke, D.J. (2022). Cell Communication

Network factor 4 promotes tumor-induced immunosuppression in melanoma. EMBO Rep. *23*, e54127. https://doi.org/10.15252/embr.202154127.

19. Ono, M., Inkson, C.A., Sonn, R., Kilts, T.M., de Castro, L.F., Maeda, A., Fisher, L.W., Robey, P.G., Berendsen, A.D., Li, L., et al. (2013). WISP1/CCN4: a potential target for inhibiting prostate cancer growth and spread to bone. PLoS One *8*, e71709. https://doi.org/10.1371/journal.pone.0071709.

20. Chang, A.C., Lin, L.W., Chen, Y.C., Chen, P.C., Liu, S.C., Tai, H.C., Wu, H.C., Sung, S.Y., Lin, T.H., and Tang, C.H. (2023). The ADAM9/WISP-1 axis cooperates with osteoblasts to stimulate primary prostate tumor growth and metastasis. Int. J. Biol. Sci. *19*, 760–771. https://doi.org/10.7150/ijbs.77495.

21. Farré, D., Roset, R., Huerta, M., Adsuara, J.E., Roselló, L., Albà, M.M., and Messeguer, X. (2003). Identification of patterns in biological sequences at the ALGGEN server: PROMO and MALGEN. Nucleic Acids Res. *31*, 3651–3653. https://doi.org/10.1093/nar/gkg605.

22. Hallett, R.M., Bonfill-Teixidor, E., Iurlaro, R., Arias, A., Raman, S., Bayliss, P., Egorova, O., Neva-Alejo, A., McGray, A.R., Lau, E., et al. (2023). Therapeutic Targeting of LIF Overcomes Macrophage-mediated Immunosuppression of the Local Tumor Microenvironment. Clin. Cancer Res. *29*, 791–804. https://doi.org/10.1158/1078-0432.Ccr-21-1888.

23. Berraondo, P., Sanmamed, M.F., Ochoa, M.C., Etxeberria, I., Aznar, M.A., Pérez-Gracia, J.L., Rodríguez-Ruiz, M.E., Ponz-Sarvise, M., Castañón, E., and Melero, I. (2019). Cytokines in clinical cancer immunotherapy. Br. J. Cancer *120*, 6–15. https://doi.org/10.1038/s41416-018-0328-y.

24. Ferguson, A., Bhinder, B., Conteduca, V., Sigouros, M., Sboner, A., Nanus, D.M., Tagawa, S.T., Rickman, D., Elemento, O., and Beltran, H. (2019). Immunogenomic landscape of neuroendocrine prostate cancer (NEPC). J. Clin. Oncol. *37*, 224. https://doi.org/10.1200/JCO.2019.37.7_suppl.224.

25. Pascual-Garcia, M., Bonfill-Teixidor, E., Planas-Rigol, E., Rubio-Perez, C., Iurlaro, R., Arias, A., Cuartas, I., Sala-Hojman, A., Escudero, L., Martinez-Ricarte, F., et al. (2019). LIF regulates CXCL9 in tumor-associated macrophages and prevents CD8(+) T cell tumor-infiltration impairing anti-PD1 therapy. Nat. Commun. *10*, 2416. https://doi.org/10.1038/s41467-019-10369-9.

26. Li, T., Fan, J., Wang, B., Traugh, N., Chen, Q., Liu, J.S., Li, B., and Liu, X.S. (2017). TIMER: A Web Server for Comprehensive Analysis of Tumor-Infiltrating Immune Cells. Cancer Res. *77*, e108–e110. https://doi.org/10.1158/0008-5472.CAN-17-0307.

27. Waugh, D.J.J., and Wilson, C. (2008). The interleukin-8 pathway in cancer. Clin. Cancer Res. *14*, 6735–6741. https://doi.org/10.1158/1078-0432.Ccr-07-4843.

28. Zhang, W., Wang, H., Sun, M., Deng, X., Wu, X., Ma, Y., Li, M., Shuoa, S.M., You, Q., and Miao, L. (2020). CXCL5/CXCR2 axis in tumor microenvironment as potential diagnostic biomarker and therapeutic target. Cancer Commun. *40*, 69–80. https://doi.org/10.1002/cac2.12010.

29. Wei, L., Liu, Y., Ma, Y., Ding, C., Zhang, H., Lu, Z., Gu, Z., and Zhu, C. (2019). C-X-C

chemokine receptor 2 correlates with unfavorable prognosis and facilitates malignant cell activities via activating JAK2/STAT3 pathway in non-small cell lung cancer. Cell Cycle *18*, 3456–3471. https://doi.org/10.1080/15384101.2019.1689471.

30. Yu, H., Pardoll, D., and Jove, R. (2009). STATs in cancer inflammation and immunity: a leading role for STAT3. Nat. Rev. Cancer *9*, 798–809. https://doi.org/10.1038/nrc2734.

31. Timofeeva, O.A., Chasovskikh, S., Lonskaya, I., Tarasova, N.I., Khavrutskii, L., Tarasov, S.G., Zhang, X., Korostyshevskiy, V.R., Cheema, A., Zhang, L., et al. (2012). Mechanisms of unphosphorylated STAT3 transcription factor binding to DNA. J. Biol. Chem. *287*, 14192–14200. https://doi.org/10.1074/jbc.M111.323899.

32. Qin, H.R., Kim, H.J., Kim, J.Y., Hurt, E.M., Klarmann, G.J., Kawasaki, B.T., Duhagon Serrat, M.A., and Farrar, W.L. (2008). Activation of signal transducer and activator of transcription 3 through a phosphomimetic serine 727 promotes prostate tumorigenesis independent of tyrosine 705 phosphorylation. Cancer Res. *68*, 7736–7741. https://doi.org/10.1158/0008-5472.Can-08-1125.

33. Faugeroux, V., Pailler, E., Oulhen, M., Deas, O., Brulle-Soumare, L., Hervieu, C., Marty, V., Alexandrova, K., Andree, K.C., Stoecklein, N.H., et al. (2020). Genetic characterization of a unique neuroendocrine transdifferentiation prostate circulating tumor cell-derived eXplant model. Nat. Commun. *11*, 1884. https://doi.org/10.1038/s41467-020-15426-2.

34. Davis, S.M., and Pennypacker, K.R. (2018). The role of the leukemia inhibitory factor receptor in neuroprotective signaling. Pharmacol. Ther. *183*, 50–57. https://doi.org/10.1016/j.pharmthera.2017.08.008.

35. Taylor, B.S., Schultz, N., Hieronymus, H., Gopalan, A., Xiao, Y., Carver, B.S., Arora, V.K., Kaushik, P., Cerami, E., Reva, B., et al. (2010). Integrative genomic profiling of human prostate cancer. Cancer Cell *18*, 11–22. https://doi.org/10.1016/j.ccr.2010.05.026.

36. Cancer Genome Atlas Research Network (2015). The Molecular Taxonomy of Primary Prostate Cancer. Cell *163*, 1011–1025. https://doi.org/10.1016/j.cell.2015.10.025.

37. Subramanian, A., Tamayo, P., Mootha, V.K., Mukherjee, S., Ebert, B.L., Gillette, M.A., Paulovich, A., Pomeroy, S.L., Golub, T.R., Lander, E.S., and Mesirov, J.P. (2005). Gene set enrichment analysis: a knowledge-based approach for interpreting genome-wide expression profiles. Proc. Natl. Acad. Sci. USA *102*, 15545–15550. https://doi.org/10.1073/pnas.0506580102.

38. Beltran, H., Prandi, D., Mosquera, J.M., Benelli, M., Puca, L., Cyrta, J., Marotz, C., Giannopoulou, E., Chakravarthi, B.V.S.K., Varambally, S., et al. (2016). Divergent clonal evolution of castration-resistant neuroendocrine prostate cancer. Nat. Med. *22*, 298–305. https://doi.org/10.1038/nm.4045.

39. Fan, Y., Yue, J., Xiao, M., Han-Zhang, H., Wang, Y.V., Ma, C., Deng, Z., Li, Y., Yu, Y., Wang, X., et al. (2017). FXR1 regulates transcription and is required for growth of human cancer cells with TP53/FXR2 homozygous deletion. Elife *6*, e26129. https://doi.org/10.7554/eLife.26129.

STAR★METHODS

KEY RESOURCES TABLE

REAGENT or RESOURCE	SOURCE	IDENTIFIER
Antibodies		
CXCL5	ThermoFisher	710010
CXCR2	Abcam	ab217314
CHGA	Cell signaling	Cat#85798
SOX2	NOVUS	NB110-37235
LIF	Cloud	PAA085Hu01
p-STAT3	Cell signaling	Cat#9145
LIFR	Proteintech	22779-1-AP
STAT3	Cell signaling	Cat#9139
PDL1	Proteintech	66248-1-Ig
WISP1	ThermoFisher	PA5-106451
ENO2	Abcam	ab218388
β-actin	Merck	MAB1501
Biological samples		
Serum samples collected from benign prostatic hyperplasia	Taipei Medical University-Affiliated Hospital	N202103136
Serum samples collected from hormone-sensitive prostate cancer	Taipei Medical University-Affiliated Hospital	N202103136
Serum samples collected from metastatic CRPC	Taipei Medical University-Affiliated Hospital	N202103136
Chemicals, peptides, and recombinant proteins		
Dihydrotestosterone	Sigma	521-18-6
charcoal-stripped serum	ThermoFisher	12676–029
CXCL5 recombinant protein	R&D Systems	254-XB
LIF recombinant protein	R&D Systems	7734-LF
X-tremeGENE HP DNA Transfection Reagent	Sigma-Aldrich	6366236001
Navarixin	Selleckchem	S8506
EC330	MedChemExpress	HY-100949
Critical commercial assays		
Mycoplasma PCR Detection Kit	Omicsbio	G238
RNeasy Midi Kit	Qiagen	74004
iScriptTM cDNA Synthesis Kit	Bio-Rad	1708890
iTaq Universal SYBR Green Supermix	Bio-Rad	1725120
RIPA buffer	ThermoFisher Scientific	8900
Matrigel matrix	Corning	354234
EZ-Magna ChIP IP Kit	Sigma-Aldrich	17–10086
human WISP1 ELISA kit	Elabscience	Cat#E-EL-H5542
Deposited data		
Human Prostate Adenocarcinoma transcriptome profiles	TCGA	https://www.cancer.gov/ccg/research/genome-sequencing/tcga

(Continued on next page)

Continued

REAGENT or RESOURCE	SOURCE	IDENTIFIER
Genomic data comparing normal prostate and prostate tumor from Taylor cohorts	Taylor et al.	https://www.ncbi.nlm.nih.gov/geo/query/acc.cgi?acc=GSE21032
Experimental models: Cell lines		
LNCaP (C-33)	ATCC	CRL-1740
C4-2	ATCC	CRL-3314
22Rv1	ATCC	CRL-2505
PC3	ATCC	CRL-3471
LASCPC-01	ATCC	CRL-3356
WMPY-1	ATCC	CRL-2854
Experimental models: Organisms/strains		
Mouse: BALB/c Nude:CAnN.Cg-Foxn1nu/CrlNarl	National Laboratory Animal Center	RMRC12005
Oligonucleotides		
ON-TARGETplus SMARTpool NC siRNA	Thermo Scientific Dharmacon	D-001810
ON-TARGETplus SMARTpool WISP1 siRNA	Thermo Scientific Dharmacon	L-010555
Primers for promoter reporter, see Table S1	This paper	N/A
Primers for RT-qPCR, see Table S2	This paper	N/A
Primers for ChIP assay, see Table S4	This paper	N/A
Recombinant DNA		
pCDH-CMV-CXCL5-EF1-Puro	System Biosciences	CD510B-1
pCDH-CMV-LIF-EF1-Puro	System Biosciences	CD510B-1
pLKO-Puro	RNAi Core Lab	TRC005
pLKO-LIFR-Puro	RNAi Core Lab	TRCN0000065616
pGreenFire1-ISRE	System Biosciences	TR016PA-P
Software and algorithms		
FACSDiva software	BD Biosciences	V6
SPSS software	IBM	Version 18.0
GraphPad Prism software	GraphPad Software	Version 8.0
GSEA software	UC San Diego and Broad Institute	https://www.gsea-msigdb.org/gsea/index.jsp
ChIP sequencing analysis	Genome Browser	https://genome.ucsc.edu
Immune cell association analysis	TIMER 2.0	http://timer.cistrome.org

RESOURCE AVAILABILITY

Lead contact

Further information and requests for resources and reagents should be directed to and will be fulfilled by the lead contact, Dr. Yen-Nien Liu (liuy@tmu.edu.tw).

Materials availability

This study did not generate new unique reagents.

Data and code availability

- The differential results related to human prostate cancer clinical data are available in the TCGA database (https://www.cancer.gov/ccg/research/genome-sequencing/tcga) and GSE21032 (https://www.ncbi.nlm.nih.gov/geo/query/acc.cgi?acc=GSE21032), which provide access to the raw sequencing data.
- All GSEA analyses were conducted using the Molecular Signature Database (https://www.gsea-msigdb.org/gsea/msigdb).
- Any additional information required to reanalyze the data reported in this paper is available from the corresponding author upon request.

EXPERIMENTAL MODEL AND STUDY PARTICIPANT DETAILS

Study participants

Serum samples were obtained from 10 male patients diagnosed with benign prostatic hyperplasia (BPH), 10 male patients with hormone-sensitive PCa (HSPC), and 8 male patients with metastatic CRPC at Taipei Medical University-Affiliated Hospital (Taipei, Taiwan). The patients' ages ranged from 40 to 80. The development stages of PCa were classified as BPH, HSPC, and metastatic CRPC. All participants were Asian males. Written informed consent was obtained from all participants, and the study protocol was approved by the Taipei Medical University Joint Institutional Review Board (from January 2021 to December 2023) (approval no. N202103136), adhering strictly to the principles of the Declaration of Helsinki.

METHOD DETAILS

Cell culture, reagents, and constructs

Adenocarcinoma PCa cells, including LNCaP (C-33), C4-2, 22Rv1, and PC3, were obtained from ATCC and cultured in RPMI-1640 medium (ThermoFisher Scientific, 11875-085) supplemented with 10% fetal bovine serum (FBS; EMD Millipore, TMS-013-BKR) and 1% penicillin. NEPC-like LASCPC-01 cells were also obtained from ATCC and cultured in modified HITES medium supplemented with 10 nM hydrocortisone (Sigma-Aldrich, H0888), 0.01 mg/mL transferrin (Sigma-Aldrich), 4 mM L-glutamine (Invitrogen), 5% FBS, and 1% penicillin. Prior to the experiments, all cell lines were routinely checked for negative mycoplasma contamination using a Mycoplasma PCR Detection Kit (Omicsbio, G238) within 6 months. To simulate ADT, cells were cultured in RPMI-1640 medium containing 10% charcoal-stripped serum (CSS; ThermoFisher, 12676-029) under standard culture conditions. Treatment with the AR ligand, dihydrotestosterone (DHT), was administered at a concentration of 10 nM for a duration of 24 h. Treatment concentrations of the CXCL5 and LIF recombinant proteins were 20 and 100 ng/mL, respectively, for the indicated durations. A CXCR2 antagonist, navarixin (Selleckchem, S8506), was used at a concentration of 5 μM for 48 h. An LIF inhibitor, EC330 (MedChemExpress, HY-100949), was administered at concentrations of 35 nM for 48 h. For conditioned medium (CM) collection, human WMPY-1 stromal cells obtained from ATCC were counted, seeded in 10-cm plates at a concentration of 3×10^6 cells/mL in 10 mL RPMI medium containing 10% FBS, and incubated at 37°C with 5% CO_2. CM was collected and centrifuged at $1000 \times g$ for 5 min to remove particulates. To culture LNCaP cells with various percentages of WMPY-1 cell-CM, WMPY-1 cell-CM was prepared, and 0%, 15%, or 50% was mixed with regular LNCaP complete medium. Constitutive overexpression of *CXCL5* and *LIF* was achieved by establishing a pCDH-CMV-MCS-EF1-Puro vector (System Biosciences) encoding the full-length complementary (c)DNA of *CXCL5* and *LIF*, while an empty vector (EV) was used as a control. Knockdown (KD) of *LIFR* was achieved by infecting cells with a recombinant lentivirus carrying a human *LIFR* short hairpin (sh)RNA vector (RNAi Core Lab, Taipei, Taiwan), with a non-target control (NC) pLKO_TRC005-Puro vector used as a control. Small interfering (si)RNAs (NC and siWISP1) were obtained from ON-TARGETplus SMARTpool siRNA (D-001810 and L-010555; Thermo Scientific Dharmacon). Regulatory sequence reporters of the *LIF* and *WISP1* genes were constructed using the pGreenFire reporter (System Biosciences), and all constructs were verified by DNA sequence analysis. A complete list of primers used for construct generation is given in Table S1.

Reverse-transcription (RT) quantitative polymerase chain reaction (qPCR)

Total messenger (m)RNA was isolated using the RNeasy Midi Kit (Qiagen, 74004). One microgram of total mRNA was used for RT with an iScriptTM cDNA Synthesis Kit (Bio-Rad, 1708890). Amplification was carried out using iTaq Universal SYBR Green Supermix (Bio-Rad, 1725120) in a thermocycler. The amplification protocol included an initial incubation at 95°C for 10 min, followed by 40 cycles of denaturation at 95°C for 15 s and annealing/extension at 60°C for 1 min. All reactions were normalized to the expression of human *18S* ribosomal (r)RNA and performed in triplicate. Primer pairs used for amplification are listed in Table S2.

Western blot analysis

For the Western blot analysis, protein samples were extracted from cells using 200 μL of RIPA buffer (ThermoFisher Scientific, 8900) supplemented with a protease inhibitor (Roche, 11697498001) and phosphatase inhibitor cocktail (Roche, 4906845001). Protein concentrations were determined using the Bradford reagent (Bio-Rad, 5000006), and samples were separated by sodium dodecylsulfate-polyacrylamide gel electrophoresis (SDS-PAGE). Proteins were transferred onto polyvinylidene difluoride (PVDF) or nitrocellulose membranes (ThermoFisher Scientific), followed by blocking with 5% bovine serum albumin (BSA) in Tris-base buffer containing 0.1% Tween 20 for 1 h. Protein bands were detected using enhanced chemiluminescence (ECL) and a Western blotting detection reagent (Millipore, WBULS0100). Antibody information for Western blotting is provided in Table S3.

Migration and invasion through matrigel assay

For the migration and invasion through Matrigel assay, LNCaP cells were cultured in 50% CM collected from WPMY-1 cells expressing either *LIFR*-KD or an NC vector. In the case of LIF protein treatment, LNCaP cells were transiently transfected with either an NC or WISP1 siRNA and then pretreated with phosphate-buffered saline (PBS) or 100 ng/mL LIF recombinant protein for 48 h. For LIF inhibitor treatment, LNCaP cells were cultured in 50% CM collected from WPMY-1 cells and treated with 35 nM EC330 for 48 h. Matrigel-coated Boyden chambers with an 8-μm pore size (24 wells) were prepared by adding 200 μL of serum-free medium diluted with Matrigel matrix (Corning, 354234). The lower

chamber was filled with 600 μL of complete medium, and the entire plate was incubated under standard cell culture conditions (37°C with 5% CO_2) for 12 h to allow for invasion. Afterward, the Matrigel-coated Boyden chambers were fixed with methanol for 5 min and stained with 0.5% crystal violet for 15 min. Non-invaded cells in the chamber were removed by gentle swabbing with a cotton swab after washing with distilled water, while invaded cells remained on the underside of the membrane. The chambers were air-dried at room temperature, and images of migrating or invading cells on the underside of the membrane were acquired using a phase-contrast microscope (Olympus) in triplicate. The cell migration assay was conducted similarly to the invasion through Matrigel assay, but without Matrigel coating on the transwell.

Proliferation assay

For the proliferation assay, LNCaP cells were seeded in 96-well plates at a density of 3×10^3 cells/well. Cell culture was established by mixing regular LNCaP complete medium with 50% CM from WPMY-1 cells treated with DMSO or 35 nM EC330 for 5 days. In the case of *WISP1*-KD, LNCaP cells were treated with PBS or 100 ng/mL of the LIF recombinant protein, followed by transient transfection with either the NC or *WISP1* siRNA for 5 days. The proliferation rate was assessed every 24 h for a period of 5 days. Cells were stained daily with 0.5% crystal violet for 15 min, followed by four washes with distilled water and subsequent drying. Prior to measurement, crystal violet was dissolved by adding 100 μL of 50% ethanol containing 0.1 M sodium citrate to each well, with gentle shaking to ensure complete dissolution. Absorbance readings at two wavelengths of 540 and 405 nm were obtained using a microplate reader. Multiple wells were used at each time point, and average values were recorded for further analysis.

Sphere-formation assay

For the sphere-formation assay, LNCaP cells were prepared by mixing regular LNCaP complete medium with 50% CM from WPMY-1 cells treated with either dimethyl sulfoxide (DMSO) or 35 nM EC330 for 1 week at a 1:1 ratio. In the case of *WISP1*-KD, LNCaP cells were transiently transfected with either the NC or *WISP1* siRNA and treated with either PBS or 100 ng/mL of the LIF recombinant protein for 1 week in complete medium. A density of 500 cells/well was combined with the desired amount of standard Matrigel matrix (Corning, 354234), the mixture was added to the bottom edge of a six-well plate, and it was allowed to incubate overnight for aggregation. Tumor spheres in each well were observed, photographed with a phase-contrast microscope (Olympus), and quantified.

Chromatin immunoprecipitation (ChIP) assay

The ChIP assay was performed using an EZ-Magna ChIP IP Kit (Sigma-Aldrich, 17–10086) following the manufacturer's protocol. Human stromal WPMY-1 cells or LNCaP cells were treated with either PBS or 100 ng/mL of the LIF recombinant protein, followed by treatment with 10 or 35 nM EC330 for 48 h. After the treatment period, cells were fixed with 1% paraformaldehyde in complete medium for 10 min, and fixation was stopped by incubating cells with 125 mM glycine buffer for 5 min. Fixed cells were washed with cold PBS containing protease and phosphatase inhibitors and then scraped under PBS buffer to collect cellular debris. Chromatin fragments of approximately 150 bp were obtained by sonication using the assay buffer provided in the kit. Immunoprecipitation of chromatin protein complexes was performed using 10 ng of an anti-phosphorylated (p)-STAT3 antibody (Sigma-Aldrich, 06–680) or normal immunoglobulin G (IgG) as a negative control (Santa Cruz, sc-2027), along with protein A-coated magnetic beads. After heat inactivation, chromatin was released from the complex using proteinase K (Sigma-Aldrich, 124568) and subsequently analyzed by an RT-qPCR. ChIP antibodies and qPCR primers used in the assay are listed in Table S4.

Promoter reporter assay

The gamma interferon activation site (GAS) element of the human *LIF* gene, located on chromosome 22 at positions 30245333 (*LIF*/GAS1: −5115), 30245856 (*LIF*/GAS2: −4592), 30248971 (*LIF*/GAS3: −1478), 30249728 (*LIF*/GAS4: −721), and 30249753 (*LIF*/GAS5: −696) in the GRCh38 reference genome, were investigated. Similarly, GASs of the human *WISP1* gene, located on chromosome 8 at positions 133189340 (*WISP1*/GAS1: −1700), 133197398 (*WISP1*/GAS2: +6357), and 133198213 (*WISP1*/GAS3: +7172) in GRCh38, were studied. To study the regulatory effects of these sequences, they were inserted into a green fluorescent protein (GFP) reporter vector (pGreenFire1-ISRE Lentivector; System Biosciences, TR016PA-P). To assess the functionality of the wild-type (WT) or mutant (M) GAS constructs, they were transiently transfected into WMPY-1 or LNCaP cells using the X-tremeGENE HP DNA Transfection Reagent (Sigma-Aldrich, 6366236001). Following transfection, cells were treated with either PBS or 100 ng/mL of the LIF protein, followed by treatment with 35 nM EC330 for 48 h. Promoter activity was evaluated using fluorescence-activated cell sorting (FACS, BD Biosciences), and relative mean fluorescent intensity (MFI) values of GFP were measured using FACSDiva software (BD Biosciences). These values were then normalized to the vehicle control. Three independent experiments were performed with triplicate samples. Primers used to generate the GAS mutant constructs of the human *LIF* and *WISP1* genes are listed in Table S1.

Enzyme-linked immunosorbent assay (ELISA)

Serum samples were collected from 10 patients with benign prostatic hyperplasia (BPH), 10 patients with hormone-sensitive PCa (HSPC), and 8 patients with metastatic CRPC at Taipei Medical University-Affiliated Hospital (Taipei, Taiwan). All patients provided written informed consent, and the study protocol was approved by the Taipei Medical University Joint Institutional Review Board (approval no. N202103136) and adhered to the principles of the Declaration of Helsinki. After blood collection, whole-blood tubes were allowed to clot for 30 min, and serum was then centrifuged at 1000 ×*g* for 20 min to remove any clotting particles. Similarly, cell culture supernatants were also centrifuged at

1000 ×*g* for 20 min to remove particles. The obtained serum samples were divided into aliquots and stored at −80°C until further use by undergoing two freeze-thaw cycles. Protein levels of WISP1 were quantified using a human WISP1 ELISA kit (Elabscience, #E-EL-H5542) following the manufacturer's instructions. Optical densities (ODs) of each standard, control, and sample were determined by subtracting the average zero-standard OD from the average of duplicate readings. A standard curve was generated using software capable of constructing a four-parameter logistic fit curve, and WISP1 protein levels in samples were calculated based on this curve.

Tumorigenicity assays in mice

The animal experimental procedures complied with the Council of Agriculture, Executive Yuan, Taiwan's Guidelines for Care and Use of Laboratory Animals. The Taipei Medical University Institutional Animal Care and Use Committee approved these procedures under approval ID: LAC-2021-0111, which encompassed the research objectives, methodologies, experimental protocols, and data handling procedures to ensure adherence to ethical standards and regulations for animal welfare. In a double-blind setup, we acquired four 6-week-old male nude mice (BALB/c Nude:CAnN.Cg-Foxn1nu/CrlNarl) from the National Laboratory Animal Center, Taipei, Taiwan. These mice were maintained in an environment controlled for temperature (20°C–26°C), humidity (30–70%), and lighting (12-h light/12-h dark cycles) to preserve their circadian rhythms and overall well-being. Each mouse in the experimental groups received a subcutaneous injection of 2×10^6 C4-2/EV or C4-2/CXCL5 cells into the right flank, with the cells suspended in 100 μL of a 50% Matrigel matrix and 50% complete medium mixture. For the EC330 treatment, mice injected with C4-2/CXCL5 cells were administered 2.5 mg/kg EC330 or DMSO as a control through intraperitoneal injection bi-daily for one month. We monitored tumor sizes and mouse body weights weekly over eight weeks. Tumor volume (V) was determined using the formula V = 0.5236 × H × W × L, where H, W, and L are the tumor's height, width, and length, respectively.

Immunohistochemical (IHC) staining

For the IHC analysis targeting CXCL5, CXCR2, LIF, WISP1, and ENO2, tumors were collected two months post subcutaneous injection of either C4-2/EV or C4-2/CXCL5 cells into mice, followed by DMSO or EC330 treatments. Prior to the IHC staining, the tumor sections were subjected to deparaffinization, rehydration, and heat-induced epitope retrieval processes. The staining protocol involved applying specific primary antibodies against proteins such as CXCL5, CXCR2, LIF, WISP1, and ENO2, detailed in Table S5. This was followed by the application of a washing solution containing Tris-buffered saline (TBS) with 0.1% Triton X-100, enhancement with avidin, and visualization with 3.3′-diaminobenzidine. After washing, the sections were counterstained with a secondary antibody, dried, and mounted in glycerol. For histomorphometric analysis, ten bright-field images of the IHC-stained sections from each specimen were captured using a phase-contrast microscope at 200× magnification (Olympus IX73). The staining intensity of the targeted proteins was evaluated and scored as 0 (negative), 1+ (weakly positive), 2+ (moderately positive), or 3+ (strongly positive). The intensity scores, ranging from 0 to 300, were calculated using the formula: (1 × percentage of 1+ cells) + (2 × percentage of 2+ cells) + (3 × percentage of 3+ cells). Statistical analysis, including *p*-value calculations, was performed using the Chi-squared test with SPSS software version 18.0.

Dataset analysis

mRNA expression data from the GSE21032 dataset by Taylor et al.[35] and human PCa datasets from The Cancer Genome Atlas (TCGA)[36] were log2 normalized. Gene set enrichment analysis (GSEA) software developed by Subramanian et al.[37] was used, and gene signatures associated with cytokine responsiveness (Kyoto Encyclopedia and Genes and Genomes (KEGG), gene ontology (GO), and Biocarta) and NEPC responsiveness (Beltran[38] and Li[7]) were obtained from the Gene Expression Omnibus (GEO) database. These gene signatures were employed to evaluate correlations of mRNA levels of *CXCL5*, *CXCR2*, *LIF*, *IL-6*, chemokine ligand 21 (*CCL21*), *CCL4*, *CCL3*, colony-stimulating factor 3 (*CSF3*), and *WISP1* with downloaded PCa datasets from TCGA. Normalized enrichment scores (NESs) and false discovery rates (FDRs) were calculated using the GSEA program. Cutoff values were determined to classify patients into high or low expression groups for each gene, based on half the number of patients derived from the GSEA analyses. Pearson correlation analyses were performed using the GSE21032 dataset to examine associations between mRNA levels of *CXCL5* and *CXCR2* with mRNA levels of *LIF*, *IL-6*, *CCL21*, *CCL4*, *CCL3*, and *CSF3* using GraphPad Prism software. For the ChIP sequencing analysis, ChIP sequencing data from GSM2752894 and GSM2752900 by Fan et al.[39] were obtained and analyzed using the Genome Browser provided by the Genomics Institute at University of California, Santa Cruz (UCSC). To examine both negative and positive correlations between LIFR expression and the extent of immune cell infiltration in PCa, prostate adenocarcinoma (PRAD) databases from TIMER 2.0[26] were conducted. The immune cell categories under scrutiny included CAFs, M2 macrophages, regulatory T (Treg) cells, M1 macrophages, CD8+ T cells, CD4+ type 1 helper T cells, myeloid-derived suppressor cells, activated myeloid dendritic cells, natural killer (NK) cells, and NKT cells. To perform this analysis, Spearman's correlations were employed, with adjustments made for purity. Various algorithms within TIMER 2.0, including TIDE, CIBERSORT, CIBERSORT-ABS, XCELL, and QUANTISEQ, were employed to assess immune infiltration.

QUANTIFICATION AND STATISTICAL ANALYSIS

GraphPad Prism software version 8.0 was utilized to create the graphs, and results are presented as the mean ± the standard error of the mean (SEM). Statistical significance between the compared groups was determined using various statistical tests including a one-way analysis of variance (ANOVA), two-way ANOVA, two-tailed *t*-test, and Bonferroni post-hoc test. A *p* value of <0.05 was considered statistically significant. All experiments were conducted independently at least three times.